Applied Energy 334 (2023) 120697

Contents lists available at ScienceDirect

Applied Energy

journal homepage: www.elsevier.com/locate/apenergy

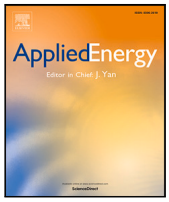

A hierarchical two-level MILP optimization model for the management of grid-connected BESS considering accurate physical model

Riccardo Nebuloni [a,*], Lorenzo Meraldi [b], Cristian Bovo [c], Valentin Ilea [a], Alberto Berizzi [a], Snigdh Sinha [a], Raviteja Bharadwaj Tamirisakandala [a], Pietro Raboni [b]

[a] Department of Energy, Politecnico di Milano, Via Lambruschini 4, Milan, 20156, Italy
[b] NHOA ENERGY, Via Privata Anton Francesco Grazzini 14, Milan, 20158, Italy
[c] Department of Electrical, Computer and Biomedical Engineering, Universita' di Pavia, Via Adolfo Ferrata 5, Pavia, 27100, Italy

ARTICLE INFO

The author Riccardo Nebuloni wants to dedicate this manuscript to his grandmother Bianca Mezzanzanica, who would have loved to see it published

Keywords:
Battery degradation
BESS
EMS
MILP
Stress factors
Variable efficiency

ABSTRACT

This work proposes a new Energy Management System (EMS) for Battery Energy Storage Systems (BESS). The goal is to make a BESS profitable in the new environment considering massive use of batteries that can be foreseen in the next future, due to the predictive increase of clean energy resources. The developed EMS considers two levels of optimization. The first level models the participation of the BESS in an Ancillary Service Market and schedules the BESS. The second level, the most innovative, is responsible for optimally distributing the power set-points obtained previously among the various battery banks considering, in addition to the battery aging, also the different efficiencies of battery banks, converters, and transformers. Moreover, this second-level manages both active and reactive power flows, and losses. Both optimization algorithms have been modeled as Mixed Integer Linear Programming (MILP) and implemented in GAMS using CPLEX as a solver. The results are encouraging: compared with the common industrial practice in which the load profile is equally shared among the individual batteries within a BESS, the two new proposed EMS strategies guarantee for a long period of operation (10-years) a consistent reduction in the number of batteries replacement (around 47%), thus ensuring significant cost savings. Moreover, the proposed BESS model accurately approximates the real physical behavior of the system, leading to an average error in State-of Energy (SoE) evaluation below 0.6%, which is almost one order of magnitude lower than the ones obtained by simpler models from literature with degradation only SoE-dependent.

1. Introduction

1.1. State of art and goals

The need for an energy transition towards clean and sustainable resources has promoted Renewable Energy Sources (RES) during the last decade and will continue to do so in the future. The intermittency of some RES highlights the difficulty of their integration. In this framework, the usage of Battery Energy Storage Systems (BESS) will greatly benefit the RES exploitation due to their high-power capacity and fast response to frequency and voltage variations [1]; indeed, a grid-forming BESS has a response time of few milliseconds [2], while the coordinated response from the plant controller, for both grid-forming and grid-following converter-interfaced BESS is lower than 100 milliseconds [3]. Therefore, the use of an Energy Management System (EMS) that optimally dispatches the individual batteries within a BESS by accurately considering their physical characteristics (degradation, variable efficiencies) to extend BESS lifetime while fulfilling BESS role within the power systems is becoming crucial. This is even more important nowadays, since BESS are assumed to provide not only a balancing of RES uncertainties, but many other services related to security of power system with a large RES integration (frequency regulation, synthetic inertia, grid forming, etc.); in the future, therefore, a more intensive use of BESS is expected, that will lead to a significant degradation of performances and reduction of BESS lifetime [4]. Hence, in the present paper, the goal is to provide an optimization model for BESS plant operation considering an accurate representation of the BESS physical model, in particular capacity degradation and loss of efficiency.

Lithium-ion (Li-ion) batteries are accepted energy storage technologies due to their high energy density and Coulombic efficiency. The capacity of Li-ion batteries fades over time due to degradation processes

* Corresponding author.
E-mail address: riccardo.nebuloni@polimi.it (R. Nebuloni).

https://doi.org/10.1016/j.apenergy.2023.120697
Received 25 May 2022; Received in revised form 22 December 2022; Accepted 13 January 2023
Available online 20 January 2023

Nomenclature

First level: Sets

t	Set of time
Δt^{BSP}	Subset of t defining the periods when an upward offer must be submitted to the market

First level: Parameters*

$\tilde{\alpha}$	Battery capacity lost due to SEI formation [–]
$\tilde{\beta}$	SEI film ratio [–]
$\tilde{\Delta t}$	Time interval [h]
$\tilde{\eta}^{chg}$	Battery charging efficiency [%]
$\tilde{\eta}^{conv}$	Converter efficiency [%]
$\tilde{\eta}^{dis}$	Battery discharging efficiency [%]
$\tilde{\eta}^{tr}$	Transformer efficiency [%]
$\overline{\tilde{CR}}$	Maximum CR [h^{-1}]
$\overline{\tilde{DoD}}$	Maximum value of DoD [–]
$\tilde{\overline{d}}^{DoD}$	Maximum value of DoD stress factor [–]
$\tilde{\overline{d}}^{id}$	Maximum value of idle degradation [–]
$\tilde{\overline{d}}^{op}$	Maximum value of operating degradation [–]
$\tilde{\overline{E}}$	Battery maximum energy capacity [MWh]
$\tilde{\overline{P}}^{chg}$	Battery maximum charging power [MW]
$\tilde{\overline{P}}^{PoC}$	Maximum power at PoC [MW]
$\overline{\tilde{SoE}}$	Battery maximum SoE [pu]
$\tilde{\pi}_t^{buy,ASM}$	ASM purchase price at time t [€]
$\tilde{\pi}_t^{buy,BM}$	BM purchase price at time t [€]
$\tilde{\pi}_t^{buy}$	Purchase price at time t [€]
$\tilde{\pi}_t^{sell,ASM}$	ASM selling price at time t [€]
$\tilde{\pi}_t^{sell,BM}$	BM selling price at time t [€]
$\tilde{\pi}_t^{sell}$	Selling price at time t [€]
$\underline{\tilde{P}}^{chg}$	Battery minimum discharging power [MW]
$\underline{\tilde{SoE}}$	Battery minimum SoE [pu]
$\tilde{AQ}$	Accepted Quantity [MW]
$\tilde{CR}^{ref}$	Reference CR [h^{-1}]
$\tilde{C}^{bat}$	Cost of the battery [€]
$\tilde{K}^{\delta_{1,2,3}}$	DoD stress factors coefficients [–]
$\tilde{K}^{CR}$	CR stress factor coefficient [–]
$\tilde{K}^{SoE}$	SoE stress factor coefficient [–]
$\tilde{K}^{Temp}$	Temperature stress factor coefficient [–]
$\tilde{K}^{time}$	Time stress factor coefficient [–]
$\tilde{L}^{init}$	Battery initial life [%]
$\tilde{MP}_t^{ASM}$	Maximum equivalent power to purchase the quantity P$\tilde{A}t$ from ASM at time t [MW]
$\tilde{MP}_t^{BM}$	Maximum equivalent power to purchase the quantity P$\tilde{A}t$ from BM at time t [MW]
$\tilde{MS}_t^{ASM}$	Maximum equivalent power to sell the quantity P$\tilde{A}t$ to ASM at time t [MW]
$\tilde{MS}_t^{BM}$	Maximum equivalent power to sell the quantity P$\tilde{A}t$ to BM at time t [MW]
$\tilde{m}^{LL,new}$	Slope of life loss function for a new battery [–]
$\tilde{m}^{LL,old}$	Slope of life loss function for an old battery [–]
$\tilde{m}^{LL}$	Slope of life loss function [–]
$\tilde{N}^{cy}$	Maximum number of cycles at maximum DoD [–]
$\tilde{n}^{cy}$	Number of cycles [–]
$\tilde{N}^{int}$	Number of time intervals contained in two hours [–]
$\tilde{SoE}^{ref}$	Reference SoE [pu]

First level: Variables

BRL_t	Battery remaining life at time t [%]
C_t^d	Battery degradation cost at time t [€]
CR_t	Battery C-rate at time t [h^{-1}]
d_t^{CR}	CR stress factor at time t [–]
d_t^{DoD}	DoD stress factor at time t [–]
d_t^{id}	Battery idle degradation at time t [–]
d_t^{op}	Battery operational degradation at time t [–]
d_t^{SoE}	SoE stress factor at time t [–]
d_t^{Temp}	Temperature stress factor at time t [–]
d_t^{time}	Time stress factor at time t [–]
d_t	Battery degradation at time t [–]
DoD_t	Battery depth-of-discharge at time t [pu]
$DQ_t^{d^{SoE},d^{CR}}$	Square of the difference between SoE stress factor and CR stress factor at time t [–]
E_t	Battery energy at time t [MWh]
$f^{d,n}$	Cycling aging test data [%]
$f^{d,t}$	Calendar aging test data [%]
L_t^{id}	Life loss in idle condition at time t [%]
L_t^{op}	Life loss in operating condition at time t [%]
L_t	Battery life loss at time t [%]
$P_t^{chg,conv}$	Converter charging power at time t [MW]
$P_t^{chg,PoC,ASM}$	Charging power at PoC from ASM at time t [MW]
$P_t^{chg,PoC,BM}$	Charging power at PoC from BM at time t [MW]
$P_t^{chg,PoC}$	Charging power at PoC at time t [MW]
P_t^{chg}	Battery charging power at time t [MW]
$P_t^{dis,conv}$	Converter discharging power at time t [MW]
$P_t^{dis,PoC,ASM}$	Discharging power at PoC to ASM at time t [MW]
$P_t^{dis,PoC,BM}$	Discharging power at PoC to BM at time t [MW]
$P_t^{dis,PoC}$	Discharging power at PoC at time t [MW]
P_t^{dis}	Battery discharging power at time t [MW]
Pr_t	Profits at time t [€]
R_t	Revenues at time t [€]
SoE_t	State of energy of battery at time t [pu]
$SQ_t^{d^{SoE},d^{CR}}$	Square of the sum of SoE stress factor and CR stress factor at time t [–]

occurring alongside the main electrochemical reactions [5], reducing their lifetime. Moreover, the efficiency also decades during operation cycling and leads to a drop in power performances [6]. Hence, both accurate capacity degradation and efficiency models are important for optimal battery operation and to assess correctly the economic feasibility of a BESS system.

Last, as far as the authors know, the industrial common practice of the BESS plant owners does not apply any optimization strategy to define the scheduling of single batteries: usually, the EMS distributes

$Z_t^{buy,ASM}$	Binary variable equal to 1 when the system purchases energy from ASM at time t
$Z_t^{buy,BM}$	Binary variable equal to 1 when the system purchases energy from BM at time t
Z_t^{chg}	Binary variable equal to 1 when the battery is charging at time t
Z_t^{dis}	Binary variable equal to 1 when the battery is discharging at time t
Z_t^{id}	Binary variable equal to 1 when the battery is in idle condition at time t
Z_t^{op}	Binary variable equal to 1 when the battery is in operating condition at time t
$Z_t^{sell,ASM}$	Binary variable equal to 1 when the system sells energy to ASM at time t
$Z_t^{sell,BM}$	Binary variable equal to 1 when the system sells energy to BM at time t

Second level: Sets

c	Set of clusters
s	Set of batteries
t	Set of time

Second level: Parameters

$\tilde{\alpha}_s$	Capacity lost due to SEI formation of battery s [–]
$\tilde{\beta}_s$	SEI film ratio of battery s [–]
$\tilde{\Delta t}$	Time interval [h]
$\tilde{\gamma}', \tilde{\xi}', \tilde{\lambda}'$	Converter losses parameters [–]
$\tilde{E}_s$	Maximum energy capacity of battery s [MWh]
$\tilde{L}_s^{init}$	Initial life of battery s [%]
$\tilde{P}_c^{fe}$	Iron losses of transformer c [MW]
$\tilde{P}_t^{PoC}$	Active power at PoC at time t [MW]
$\tilde{Q}_c^{hyst}$	Hysteresis losses of transformer c [MVAr]
$\tilde{Q}_t^{PoC}$	Reactive power at PoC at time t [MVAr]
$\tilde{R}_c^{s,tr}$	Series resistance of transformer c [Ω]
$\tilde{SoH}_s^f$	State of health resistance growth factor of battery s [–]
$\tilde{V}_c^{n,sec}$	Secondary side nominal voltage of transformer c [kV]
$\tilde{V}_s$	Nominal voltage of battery s [kV]
$\tilde{X}_c^{s,tr}$	Series reactance of transformer c [Ω]

Second level: Variables

$\eta_{c,t}^{tr}$	Efficiency of transformer c at time t [%]
$A_{s,t}^{conv}$	Apparent power through converter s at time t [MVA]
$BRL_{s,t}$	Battery remaining life of battery s at time t [%]
$CR_{s,t}^2$	Square of CR of battery s at time t [h^{-2}]
D_t^{obj}	Second level objective variable [–]
$d_{s,t}$	Degradation of battery s at time t [–]
$DQ_{s,t}^{R^{bat},CR^2}$	Square of the difference between battery resistance and square of CR for battery s at time t [–]
$I_{s,t}^{conv}$	Current through converter s at time t [A]
$I_{c,t}^{sec'}$	Series current at the secondary side of transformer c at time t [A]
$L_{s,t}$	Life loss of battery s at time t [%]
$P_{c,t}^{chg,tr,sec}$	Active charging power at secondary side of transformer c at time t [MW]
$P_{c,t}^{dis,tr,sec}$	Active discharging power at secondary side of transformer c at time t [MW]
$P_{c,t}^{joule,tr}$	Joule losses of transformer c at time t [MW]
$P_{s,t}^{loss,bat}$	Joule losses of battery s at time t [MW]
$P_{s,t}^{loss,conv}$	Losses of converter s at time t [MW]
$P_{c,t}^{tr,prim}$	Active power at primary side of transformer c at time t [MW]
$P_{c,t}^{tr,sec}$	Active power at secondary side of transformer c at time t [MW]
$Q_{c,t}^{chg,tr,sec}$	Reactive charging power at secondary side of transformer c at time t [MVAr]
$Q_{c,t}^{dis,tr,sec}$	Reactive discharging power at secondary side of transformer c at time t [MVAr]
$Q_{c,t}^{flux,tr}$	Magnetic flux losses of transformer c at time t [MVAr]
$Q_{c,t}^{tr,prim}$	Reactive power at primary side of transformer c at time t [MVAr]
$Q_{c,t}^{tr,sec}$	Reactive power at secondary side of transformer c at time t [MVAr]
$R_{s,t}^{bat,a}$	Resistance a of battery s at time t [Ω]
$R_{s,t}^{bat,b}$	Resistance b of battery s at time t [Ω]
$R_{s,t}^{bat}$	Resistance of battery s at time t [Ω]
$SoE_{s,t}^a$	State of energy a of battery s at time t [pu]
$SoE_{s,t}^b$	State of energy b of battery s at time t [pu]
$SoE_{s,t}$	State of energy of battery s at time t [pu]
$SQ_{s,t}^{R^{bat},CR^2}$	Square of the sum of battery resistance and square of CR for battery s at time t [–]
$Z_{s,t}^a$	Binary variable equal to 1 when the SoE of battery s at time t is lower than 0.5
$Z_{s,t}^b$	Binary variable equal to 1 when the SoE of battery s at time t is higher than 0.5
$Z_{s,t}^{op}$	Binary variable equal to 1 when the battery s is in operating condition at time t

* To facilitate reading, parameters are indicated with the symbol, whereas the variables without.

the power to be exchanged with the network evenly among them, without any prioritization. While this strategy can be acceptable in case of BESS equipped with perfectly equal batteries (same type, same aging, etc.), in case of BESS equipped with batteries of different characteristics it can lead to sub-optimal operation: the BESS overall efficiency will be lower and older batteries will need to be replaced sooner. The latter factor is very important nowadays because, as battery prices are still decreasing [7], the industrial practice tends to delay as much as possible any battery replacement. To point out the importance of this issue, it is worth mentioning the expected exploitation of second-life batteries in future BESSs, that will result in the presence of different batteries in the same BESS. Therefore, a way to optimally manage the single battery within a BESS power set-point, with the goal to delay as much as possible their replacement, while considering both capacity degradation and reduction of efficiency, is also investigated in this paper.

1.2. Bibliography review

Numerous market studies already exist in the literature with the aim of performing a short or long-term economic analysis. Due to

their fast reacting behavior, batteries have been studied within a market framework as primary frequency regulation provider [8–10], for secondary and tertiary regulation services [11,12] and for other services [13–17]. In [18] models for batteries in the Ancillary Services Market (ASM) have been presented. However, these papers focus on the services provided and model BESS in a very basic manner; none of them consider capacity degradation over lifetime whereas efficiency is assumed constant. The effects on BESS for participation to regulation services and to frequency control is shown in [19,20] respectively, where also premature aging is considered, with reference to the Italian ASM; however, neither study does optimize the BESS scheduling and aging is considered with a very simplified approach.

Detailed physical models able to capture accurately the capacity degradation phenomena are available in literature, but they are never directly used in any optimization tool for BESS operation due to their complexity and significant non-linearity. Complete physical models can be found in [21,22], that focus on semi-empirical models while suggesting temperature, State of Energy (SoE), time, C-Rate (CR), and Depth of Discharge (DoD) as the factors which affect calendar and cyclic degradation in Li-ion batteries, while also considering the Solid Electrolyte Interphase (SEI) film formation in the early period of battery life. However, optimization models considering some of the above mentioned adverse effects, in a simplified manner, can be found in the literature. In [23], capacity degradation is calculated only in a post-optimization process starting from the SoE optimized profile and using the Rainflow-Counting-Algorithm (RCA) [24] and, therefore, it is not considered for optimal scheduling of batteries. In [25], a whole-life-cycle battery model has been implemented for providing multiple functional services in power systems based on the battery remaining life; it considers a simplified degradation model based on the maximum number of cycles at a certain DoD value, ignoring the other factors. In [26,27], stochastic dynamic programming models have been investigated considering all the stress factors for the operating conditions, but ignoring idle degradation; moreover, the models are non-linear, and therefore hardly applicable to large scale problems with discrete variables. Paper [28] explores a linear optimization model describing the characteristics of several types of batteries; it describes the SoE as the main stress factor which affects the battery capacity fading. In [29], a Mixed Integer Linear Problem (MILP) degradation model is considered, but it is only DoD-dependent. Ref. [30] explores a piecewise linear function for the degradation cost based on a linear approximation of the RCA dividing battery capacity into segments for setting the energy capacity limits; however, only the DoD is considered as degradation factor. Ref. [31] proposes a MILP model in which degradation and efficiency effects are considered through an external loop that updates the parameters for the following MILP execution, therefore providing a reduced level of accuracy for the desired phenomena; moreover, the iterative process could take a long time, not suitable for operating optimization.

Concerning the reduction of battery efficiency, a physical model is explained in [32] that indicates SoE and State-of-Health (SoH) as the major factors influencing it. On the other hand, most optimization studies found in literature consider constant component efficiencies, and only a few treat them as variable over time. Paper [33] defines a cost function considering energy conversion losses and cycle-induced capacity reduction to calculate the marginal costs as a function of charging and discharging operations, therefore only CR-dependent. Ref. [34] considers a variable efficiency for the converter and battery system, but only as a function of the SoE. In [35], a trade-off between grid economics and storage health considering battery variable efficiency is studied; however, the battery internal resistance is considered constant and efficiency is assumed dependent only on CR. Therefore, these articles do not consider all the factors for decreasing efficiency listed above, but only some taken individually.

Lastly, due to the recent gradual opening in some countries of voltage support services, the reactive power flow problem has also been investigated. Papers [14,36,37] study different control strategies to deal with both active and reactive power. Here, it is shown that inverter-based operation of the BESS offers flexibility in absorbing or injecting active and/or reactive power, but, this aspect must be integrated in the physical model of BESS since the reactive power can substantially influence the losses in the BESS components (hence their efficiencies), especially in optimization studies. Regarding this last problem, the papers previously analyzed in the bibliography review do not consider the reactive power flow effects on the physical model. However, this is studied separately in articles such as [38–40] where active and reactive power flows are integrated into optimization models, but the level of modeling of the components is very simplified compared with others, which this can lead to non-efficient BESS working conditions.

1.3. Paper contribution

The lack in literature of a complete MILP model that considers all the physical aspects highlighted in [21,22,32] motivates the methodology proposed in this paper, whose aim is to define a tractable linear model for the operation of BESS considering all the aforementioned aspects. Hence, since it is necessary to define a market environment for BESS plant, it is considered BESS participates in the ASM, thus being subject to adverse effects like capacity degradation and reduction of efficiency over time. The choice of this market comes from its intrinsic structure, which guarantees a sufficient high variation in the charging and discharging profiles of the BESS. Tests of various approximation levels will show the importance of modeling all factors. To maximize the BESS profitability, the optimization procedure will first define the bids on the ASM and then share the resulting power profile among the different batteries of the BESS. In terms of representation, the BESS is modeled in detail, including all the main electrical components from the Point of Connection (PoC) to the batteries, while the representation of the external grid is neglected; the service provided to the grid is considered in terms of power profile request at PoC, which of course depend on the type of grid: distribution or transmission.

The optimization problem is therefore divided into two hierarchical levels. The first level performs an economical evaluation of profitability for the BESS participation in ASM and it gives a BESS optimal active power profile as output. Market modeling is not the focus of this paper: it depends on the type of services considered, the regulations, and could be different in different countries and for different voltage levels (distribution or transmission). For illustrative purposes, in the paper, the Italian ASM, that acts at transmission level, is considered and modeled, assuming that the BESS is operating as Virtual Power Plant (VPP), and in particular as Mixed Aggregate Virtual Units (UVAM, in Italian) [41]. The UVAM in Italy is seen by the market operator as a unique economic offer, or bid, that aggregates a mix of resources. In this paper, UVAM is considered made of BESS only, but, in general, the first level optimization problem can be extended with the constraints modeling other resources (like renewable or conventional plants, prosumers, etc.). In the latter case, the BESS profiles would be optimized together with other resources profiles, but the proposed BESS model, that is the main contribution of this paper, will not change. Therefore, the same proposed model can be used for any application, either for distribution or transmission networks, once the service to be provided is defined.

The second level deals with the distribution of the load profile resulting from the first level optimization among the single batteries which make up the BESS. At this stage, which is the main part of this study, the detailed model of capacity degradation and efficiency reduction for batteries, together with efficiency variation for converters and transformers, are considered. The second level can be optimized both in one-shot, which allows an optimal solution for the entire considered period, or through a rolling horizon optimization [42,43]. The use of the rolling horizon guarantees both shorter computation

times and greater robustness to any change of the dispatching profile and it is the solution adopted here.

The use of two hierarchical independent optimization levels allows greater flexibility of the model: in fact, the first level defines the BESS schedule based on the adopted market rules (operation environment), while the second level is independent of the type of market implemented. It is worth noticing that the optimization problem only requires information typically available to EMS operators and designers, thus adding practical industrial value to the proposed procedure.

Summarizing, the novel contributions of the paper are:

- the implementation of an optimization model for the operation of a BESS fully considering the physical models of:
  - the capacity degradation of batteries depending on SoE, CR, DoD, time as stress factors and the SEI formation in the life-loss calculation steps;
  - the optimization model proposed is a linearization of [21, 22] and is designed to minimize the use of additional integer variables and get computation times compatible with real life operation;
  - the variable efficiency model of batteries, converters, and transformers considering all physical factors that influence them (e.g., for batteries, SoE, SoH, and CR).

  While this has been enforced above, the following additional contributions can also been considered at the second level optimization side:
- an improvement of the current industrial practice, that currently shares evenly the loading among different batteries of a BESS, through the introduction of two new EMS strategies for the optimal battery set-point definition;
- the consideration in the linear optimization problem of the reactive power flows as they have a significant impact on losses, especially on converters, opening the possibility for future voltage/reactive power control strategy integration.

The rest of the paper is organized as follows: Section 2 describes the two-level optimization model as Mixed Integer Non Linear Programming (MINLP), Section 3 presents the linearization techniques to get a MILP optimization model, Section 4 summarizes the input data identification, the simulation results, and a comparison with literature models. Lastly, Section 5 highlights the conclusions.

2. Complete MINLP model

2.1. First optimization level

The goal of the first level is to define a profitable load profile for the BESS involved in the UVAM, which then will have to be optimally managed by the second level. Fig. 1 shows the scheme considered and related variables adopted for the first level; in particular, the plant equivalent converter and transformer represent the aggregate of the single components, which from a mathematical point of view are added together, and will be considered individually in the second optimization level (Fig. 2). It worth reminding that UVAM can also contain other type of resources; they can be added here considering their corresponding models and their effect would consist in additional power injections at PoC level in Fig. 1 or at the secondary side of the plant equivalent transformer. The rest of the model would be the same. In a more complex context, it is possible that UVAM is made of multiple plants of the type shown in Fig. 1. In this case, the model formulated here would characterize any one of them and their power profiles would be linked by the economic objective that would consider the sum of these profiles. In this case, decomposition techniques can be applied to efficiently solve the problem, like the Dantzig–Wolfe decomposition [44], already successfully applied in aggregator context [45].

The first level objective function is the profit maximization:

$$Max\ \tilde{\Delta t} \sum_t Pr_t = \tag{1}$$
$$= Max\ \tilde{\Delta t} \sum_t (-\tilde{\pi}_t^{sell} P_t^{dis,PoC} - \tilde{\pi}_t^{buy} P_t^{chg,PoC} - C_t^d)$$

Problem (1) optimizes the trade-off between the potential revenues that can be obtained by discharging power in the grid and the costs due to energy purchase and the degradation.

Problem (1) is subject to several constraints:

2.1.1. BESS electrochemical model

SoE evolution, considering battery efficiency, is described by (2):

$$SoE_t = SoE_{t-1} + \frac{\tilde{\Delta t}}{\tilde{E}} \left(P_t^{chg} \tilde{\eta}^{chg} + \frac{P_t^{dis}}{\tilde{\eta}^{dis}} \right) \tag{2}$$

To avoid over-charging and over-discharging, SoE is kept within a certain range, specified by the manufacturer:

$$\underline{\tilde{SoE}} \le SoE_t \le \overline{\tilde{SoE}} \tag{3}$$

Constraints (4) limit the battery charging and discharging power within their bounds, whereas (5) prevents charging and discharging at the same time, and (6) from being simultaneously in operating and idle conditions:

$$0 \le P_t^{chg} \le \overline{\tilde{P}}^{chg} Z_t^{chg} \tag{4a}$$
$$\underline{\tilde{P}}^{dis} Z_t^{dis} \le P_t^{dis} \le 0 \tag{4b}$$

$$Z_t^{chg} + Z_t^{dis} \le 1 \tag{5}$$

$$Z_t^{op} = Z_t^{chg} + Z_t^{dis} \tag{6a}$$
$$Z_t^{op} = 1 - Z_t^{id} \tag{6b}$$

The CR is the unit used to measure the speed at which a battery is fully charged or discharged; for example, charging at a CR of 1C means that the battery is charged from 0%–100% in one hour. Hence, CR is the power that would deliver the complete capacity of a battery over an hour; it can be expressed as:

$$CR_t = \frac{P_t^{chg} - P_t^{dis}}{\tilde{E}} \tag{7}$$

Power flows through the battery, converter, and transformer are expressed in (8):

$$P_t^{chg,conv} = \frac{P_t^{chg}}{\tilde{\eta}^{conv}} \tag{8a}$$
$$P_t^{dis,conv} = P_t^{dis} \tilde{\eta}^{conv} \tag{8b}$$
$$P_t^{chg,PoC} = \frac{P_t^{chg,conv}}{\tilde{\eta}^{tr}} \tag{8c}$$
$$P_t^{dis,PoC} = P_t^{dis,conv} \tilde{\eta}^{tr} \tag{8d}$$

2.1.2. Battery degradation model

Battery degradation is a very complicated process and its closed form modeling is a problem not yet completely solved [46]. However, the remaining life of battery can be described by the following experimentally validated equation [21]:

$$BRL_t = \tilde{\alpha} e^{-\tilde{\beta} d_t} + (1 - \tilde{\alpha}) e^{-d_t} \tag{9}$$

During the early period of Li-ion battery life, a SEI film is formed due to the consumption of certain number of Li-ions [47], leading to a higher degradation rate. The formation of this film stops once the SEI has stabilized and hence, the degradation rate becomes lower: in general, below 90%, the parameter $\tilde{\alpha}$ becomes 0 [21].

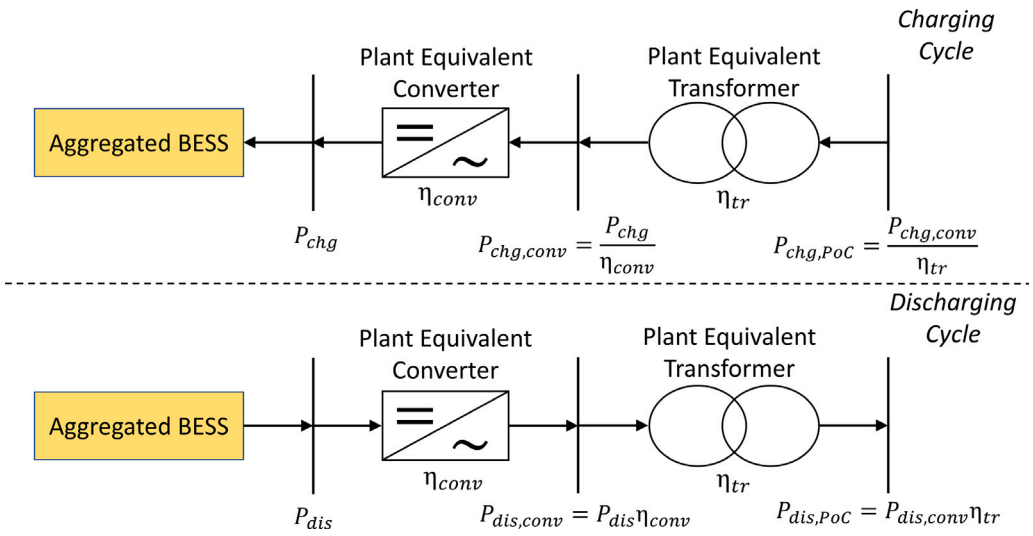

Fig. 1. Scheme of the considered first level.

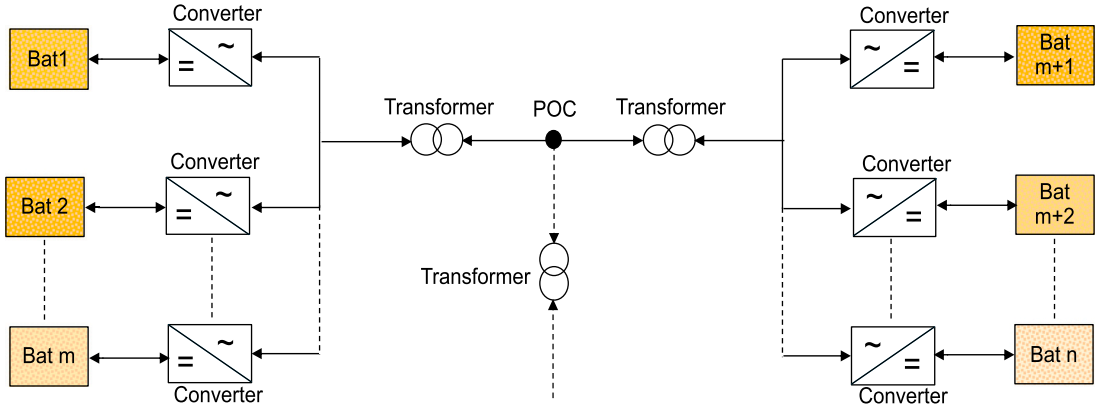

Fig. 2. Second level BESS schematic representation.

In (9), the cumulative degradation function is used to define the combined effect of the stress factors; in this model, it is distinguished between operational and idle degradation factors [48]:

$$d_t = d_t^{op} + d_t^{id} \tag{10}$$

where:

$$d_t^{op} = d_t^{time} + d_t^{CR} d_t^{DoD} d_t^{SoE} d_t^{Temp} \tag{11a}$$

$$d_t^{id} = d_t^{time} d_t^{SoE} d_t^{Temp} \tag{11b}$$

Since a battery cannot be both in idle and operating condition due to (6), at a particular time instance the effect of either d_t^{op} or d_t^{id} will be zero. Therefore, (10) can be better rewritten as:

$$d_t = d_t^{op} Z_t^{op} + d_t^{id} Z_t^{id} \tag{12}$$

The degradation cost in (1), i.e. C_t^d, can then be expressed as:

$$C_t^d = \tilde{C}^{bat} L_t \tag{13}$$

where:

$$L_t = \tilde{L}^{init} - BRL_t \tag{14}$$

By expressing the degradation cost as in (13), it is possible to evaluate the fraction of the initial investment cost "virtually" lost due to degradation; in this way, as for (1), the battery will make offers only if the operation cost is lower than the possible revenue.

The components of (11) are given by:

- **SoE stress factor**

The formula for determining the SoE stress factor of (11) is [21]:

$$d^{SoE}(SoE) = e^{\tilde{K}^{SoE}(SoE - \tilde{SoE}^{ref})} \tag{15}$$

To obtain the value of $\tilde{K}^{SoE}$, we can write that [21]:

$$\frac{d^{SoE}(\tilde{SoE}^A)}{d^{SoE}(\tilde{SoE}^{ref})} = \frac{f^{d,t}(SoE = \tilde{SoE}^A)}{f^{d,t}(SoE = \tilde{SoE}^{ref})} \tag{16}$$

where $f^{d,t}$ represents the aging data function and $\tilde{SoE}^A$ represents a generic SoE value for which the stress factor d^{SoE} is calculated. From (15), we have that:

$$d^{SoE}(SoE = \tilde{SoE}^{ref}) = 1 \tag{17}$$

and (16) becomes:

$$d^{SoE}(\tilde{SoE}^A) = \frac{f^{d,t}(SoE = \tilde{SoE}^A)}{f^{d,t}(SoE = \tilde{SoE}^{ref})} \tag{18}$$

The left-hand side of (18) was substituted in (15) and the value of $\tilde{K}^{SoE}$ was determined. The right-hand side of (18) can be determined using curve fitting technique on the calendar aging test data provided by the manufacturer.

- **CR stress factor**

The formula for determining the CR stress factors is [22]:

$$d^{CR}(CR) = e^{\tilde{K}^{CR}(CR - \tilde{CR}^{ref})} \tag{19}$$

A similar procedure used for the identification of $\tilde{K}^{SoE}$ can be adopted for $\tilde{K}^{CR}$, using cycling aging test data.

- **DoD stress factor**
  The empirical formula for DoD stress factor is [21]:

$$d^{DoD}(DoD) = \frac{1}{\tilde{K}^{\delta_1} DoD^{\tilde{K}^{\delta_2}} + \tilde{K}^{\delta_3}} \tag{20}$$

- **Time stress factor**
  The formula for time stress factor is adopted from [22]:

$$d^{t}(t) = \tilde{K}^{time} t \tag{21}$$

To obtain the value of $\tilde{K}^{time}$, similar steps as those taken for $\tilde{K}^{SoE}$ and $\tilde{K}^{CR}$ can be adopted:

$$\tilde{K}^{time} = \frac{f^{d,t}(SoE = S\tilde{o}E^{A})}{t\ d^{SoE}(S\tilde{o}E^{A})} \tag{22}$$

The values of $f^{d,t}(SoE = S\tilde{o}E^{A})$ are determined from the calendar test data and $d^{SoE}(S\tilde{o}E^{A})$ from (15).

- **Temperature stress factor**
  The formula for determining the temperature stress factors is [22]:

$$d^{Temp}(Temp) = e^{\tilde{K}^{Temp}(Temp - \tilde{Temp}^{ref})} \tag{23}$$

Similar steps followed for the identification of $\tilde{K}^{SoE}$ can be adopted for $\tilde{K}^{Temp}$, using cycling aging test data at different temperatures.

2.1.3. Market model

To simulate the participation of the BESS in a real electricity market, for illustrative purposes, the Italian UVAM case has been considered [49]. In case of a market or, more generally, a service designed differently, the equations described here could be partially, or completely, changed, without altering the proposed physical model of the BESS. The system described in Section 2.1.1 can participate in both the ASM and Balancing Market (BM) services, and can make both upwards and downwards bids (so it can both buy or sell energy) according to historical price data. In this stage, for simplification, all the bids made by the BESS are assumed to be accepted.

When the system bids on the market, the bidded quantity must be greater than or equal to the minimum Accepted Quantity (AQ), equal to 1 MW [49]:

$$\tilde{AQ} Z_t^{chg} \le P_t^{chg,PoC} \le \tilde{\overline{P}}^{PoC} Z_t^{chg} \tag{24a}$$

$$-\tilde{\overline{P}}^{PoC} Z_t^{dis} \le P_t^{dis,PoC} \le -\tilde{AQ} Z_t^{dis} \tag{24b}$$

The offer must be held for at least 2 h [49]; this commitment can be mathematically described by (25):

$$P_t^{chg,PoC,ASM} \ge P_{t-i}^{chg,PoC,ASM} - P_{t-\tilde{N}^{int}}^{chg,PoC,ASM} \tag{25a}$$

$$P_t^{chg,PoC,BM} \ge P_{t-i}^{chg,PoC,BM} - P_{t-\tilde{N}^{int}}^{chg,PoC,BM} \tag{25b}$$

$$P_t^{dis,PoC,ASM} \le P_{t-i}^{dis,PoC,ASM} - P_{t-\tilde{N}^{int}}^{dis,PoC,ASM} \tag{25c}$$

$$P_t^{dis,PoC,BM} \le P_{t-i}^{dis,PoC,BM} - P_{t-\tilde{N}^{int}}^{dis,PoC,BM} \tag{25d}$$

that represent a series of systems of inequalities in which $i = 1, \dots, \tilde{N}^{int}$, and $\tilde{N}^{int} = 2\ h$. Appendix details the mechanism of (25).

An upward offer on the BM for at least 4 consecutive hours between 2:00 pm and 8:00 pm must be submitted every day from Monday to Friday [49]; this is represented by (26):

$$P^{dis,PoC,BM}_{t \in \Delta t^{BSP}} \le -\tilde{AQ} \tag{26}$$

The objective function (1) can then be rewritten as:

$$Max\ \tilde{\Delta t} \sum_t (-\tilde{\pi}_t^{buy,ASM} P_t^{chg,PoC,ASM} + \tag{27}$$
$$-\tilde{\pi}_t^{buy,BM} P_t^{chg,PoC,BM} - \tilde{\pi}_t^{sell,ASM} P_t^{dis,PoC,ASM} +$$
$$-\tilde{\pi}_t^{sell,BM} P_t^{dis,PoC,BM} - C_t^d)$$

where C_t^d is given by (13).

Eqs. (28) split the active power at the PoC into the ASM and BM components, depending on the prices in a particular time step:

$$P_t^{chg,PoC} = P_t^{chg,PoC,ASM} + P_t^{chg,PoC,BM} \tag{28a}$$

$$P_t^{dis,PoC} = P_t^{dis,PoC,ASM} + P_t^{dis,PoC,BM} \tag{28b}$$

The maximum amount of power the system can buy or sell through the markets is set by (29):

$$P_t^{chg,PoC,ASM} \le \tilde{M} P_t^{ASM} Z_t^{buy,ASM} \tag{29a}$$

$$P_t^{chg,PoC,BM} \le \tilde{M} P_t^{BM} Z_t^{buy,BM} \tag{29b}$$

$$P_t^{dis,PoC,ASM} \le \tilde{M} S_t^{ASM} Z_t^{sell,ASM} \tag{29c}$$

$$P_t^{dis,PoC,BM} \le \tilde{M} S_t^{BM} Z_t^{sell,BM} \tag{29d}$$

Eqs. (30) guarantee that the system can only participate in one market for each time interval:

$$Z_t^{buy,ASM} + Z_t^{buy,BM} \le 1 \tag{30a}$$

$$Z_t^{sell,ASM} + Z_t^{sell,BM} \le 1 \tag{30b}$$

Finally, (31) describe the maximum number of charging and discharging cycles referred to the maximum DoD:

$$\sum_t P_t^{chg} \le \tilde{N}^{cy}(\tilde{\overline{SoE}} - \tilde{\underline{SoE}})\tilde{\overline{E}} \tag{31a}$$

$$\sum_t P_t^{dis} \ge -\tilde{N}^{cy}(\tilde{\overline{SoE}} - \tilde{\underline{SoE}})\tilde{\overline{E}} \tag{31b}$$

where:

$$\tilde{\overline{E}} = \frac{\tilde{\overline{P}}^{chg} \tilde{L}^{init}}{\tilde{\overline{CR}}} \tag{32}$$

Eq. (32) indicates that lower the initial life, lower the amount of energy that the battery can exchange during operation is.

2.1.4. Comments about the first level

For the sake of simplicity, for the first level the authors considered a variable degradation/constant efficiency model as for (8), being aware that this assumption may lead to possible error by comparing the exact non-linear model [50]. However, this choice stems from the fact that the first level could be a tool with which the aggregator dispatches an aggregate of individual plants; this possibility can lead to large problems, which is not even too unrealistic given that in Italy within a UVAM there can be several plants. There is also a "practical" problem in having the aggregator have the data from all possible merged plants available; this is because the aggregator generally does not own the BESS [51]. The choice to consider variable degradation makes it possible to use (13) to estimate the operating cost when the BESS is used. In any case, as will be shown in Section 4.3, the modeling detail proposed in the article for the second level compensates for the inaccuracies that result from the first level.

2.1.5. Summary of the first level

Considering the above equations, the first optimization level can be summarized as:

OF : (27)

$s.t.$: (2)–(9), (11)–(15), (19)–(21), (24)–(26), (28)–(32).

2.2. Second optimization level

In the second level, the BESS follows the scheduled output of the first level, whereas the EMS distributes the total power exchanged among all the batteries with the objective of minimizing their individual capacity degradation. Fig. 2 shows the scheme of the second level: batteries are assumed to be connected to their own converter and converters are assumed to be linked to a transformer. All the transformers are connected to the PoC.

To model the scheme, the following sets have been introduced:

- battery and converters variables are indexed through the *storage sets (s,t)*, since each battery bank has its own converter;
- transformers variables are indexed through the *transformer sets (c,t)*.

The second level optimization problem is described by:

$$Min\ \tilde{\Delta t} \sum_t D_t^{obj} \tag{33}$$

As stated in the Introduction, three different strategies are defined. The three strategies are characterized by the definition of D_t^{obj}:

(A) $D_t^{obj} = \sum_s L_{s,t}$: Strategy A simulates the current industrial application: the load profile is equally shared among the individual batteries of the BESS:

$$P_{s,t}^{chg} = P_{s+1,t}^{chg} \tag{34}$$

$$P_{s,t}^{dis} = P_{s+1,t}^{dis} \tag{35}$$

(B) $D_t^{obj} = \sum_s \frac{d_{s,t}}{L_s^{init}}$: Strategy B goal is to align batteries to a common SoH level. $d_{s,t}$ is a representation of the degraded conditions of the batteries, regardless of their SoH. The term L_s^{init} aims at equalizing the batteries, since it forces to use newer ones over older ones;

(C) $D_t^{obj} = \sum_s \frac{L_{s,t}}{L_s^{init}}$: in Strategy C, we integrate the life-loss variable $L_{s,t}$ in the objective function, weighting it, as in Strategy B, with L_s^{init} to favor the use of newer batteries over the old ones. The explicit presence of $L_{s,t}$ takes into account the zeroing of the parameter $\tilde{\alpha}_s$ once a battery gets older and reaches stable SEI.

The model is completed by the following constraints. Eq. (36) imposes that the overall power on PoC side is given by the sum of the powers at primary side of the transformers:

$$\tilde{P}_t^{PoC} = \sum_c P_{c,t}^{tr,prim} \tag{36a}$$

$$\tilde{Q}_t^{PoC} = \sum_c Q_{c,t}^{tr,prim} \tag{36b}$$

Eq. (36b) does not come from the first level, but it represents the imposed reactive power request from the grid, and it is treated as a given input for the second level.

From a theoretical point of view, the reactive power flow within BESS would affect the amount of active power that the BESS can exchange in the market according to the formula $P_{MAX}^2 = A_{MAX}^2 - Q^2$, a limit imposed, among others, by the capability of the converters. However, considering that currently in many countries (including Italy) there is not yet a voltage regulation service requirement, which would stimulate important amounts of reactive power to the BESS, the amount of reactive power inside the plant is mostly given by reactive losses and, hence, has small values. Therefore, a constant P_{MAX} calculated at nominal power factor has been considered, in order to cover the non-null reactive power flows.

Eqs. (37) are written for the transformers and link the secondary side active and reactive power variables to the primary ones through the efficiencies, that are now variables:

$$P_{c,t}^{tr,prim} = P_{c,t}^{chg,tr,sec}\eta_{c,t}^{tr} + \frac{P_{c,t}^{dis,tr,sec}}{\eta_{c,t}^{tr}} \tag{37a}$$

$$Q_{c,t}^{tr,prim} = Q_{c,t}^{chg,tr,sec}\eta_{c,t}^{tr} + \frac{Q_{c,t}^{dis,tr,sec}}{\eta_{c,t}^{tr}} \tag{37b}$$

$$P_{c,t}^{tr,sec} = P_{c,t}^{chg,tr,sec} + P_{c,t}^{dis,tr,sec} \tag{37c}$$

$$Q_{c,t}^{tr,sec} = Q_{c,t}^{chg,tr,sec} + Q_{c,t}^{dis,tr,sec} \tag{37d}$$

In (38), the active and the reactive power of transformers are divided among the converters connected:

$$P_{c,t}^{tr,sec} = \sum_{s\in c}(P_{s,t}^{chg,conv} + P_{s,t}^{dis,conv}) \tag{38a}$$

$$Q_{c,t}^{tr,sec} = \sum_{s\in c}(Q_{s,t}^{chg,conv} + Q_{s,t}^{dis,conv}) \tag{38b}$$

Finally, (2)–(8) in Section 2.1.1, (9)–(32) in Section 2.1.2 can be extended for the whole set of batteries. In this case, the battery efficiency is considered as a time dependent variable.

Fig. 3 summarizes the proposed complete two-levels optimization model scheme: for each day, historical price data and the initial status of the system (represented by the average values of BRL and SoE) are given as input to the first level, which determines a profitable load profile by weighting the trade-off between the degradation cost and the profits from participating in the market. The resulting profile is given as input to the second level, which define the set-points of the single batteries within the BESS by considering detailed modeling of degradation and losses; at the end of the day, information about the individual BRL and SoE are monitored as used for the following day.

2.2.1. Summary of the second level

Considering the above equations, the second optimization level can be summarized as:

OF : (33)

$s.t.$: (2)–(9), (11)–(15), (19)–(21), (32), (36)–(38).

3. Proposed MILP model

Eqs. (2), (8), (9), (11), (12), (15), (19), (20), and (37), introduced in Section 2, are non-linear, resulting, in the presence of many components, in a large MINLP model which is difficult to solve in reasonable time. For this reason, the linearization of the model is proposed in this Section and a numerically tractable MILP model is obtained, without losing the accuracy inherent to the MINLP model.

Several linearization methods exist in the literature, such as, for example, Special Order Set of Type One and Two (SOS1 and SOS2) [52], and the Constraint Cost Variable (CCV) method [53]. Many of these techniques rely on the use of many additional binary variables which can significantly increase the complexity of the MILP problem: using too many will also lead to an intractable MILP model. Instead, the CCV method does not require the introduction of additional binary variables, but it requires the non-linear function to be convex. However, as it will be clarified further, the non-linear model shown in Section 2 is not directly suited for the CCV method, as many of the functions or characteristics are not convex. Therefore, to take full advantage of the CCV method, the non-linear equations of the model have been made convex when necessary and possible.

3.1. Degradation

This subsection refers to the linearization of the first level; the same equations are valid for the second level by adding the set s.

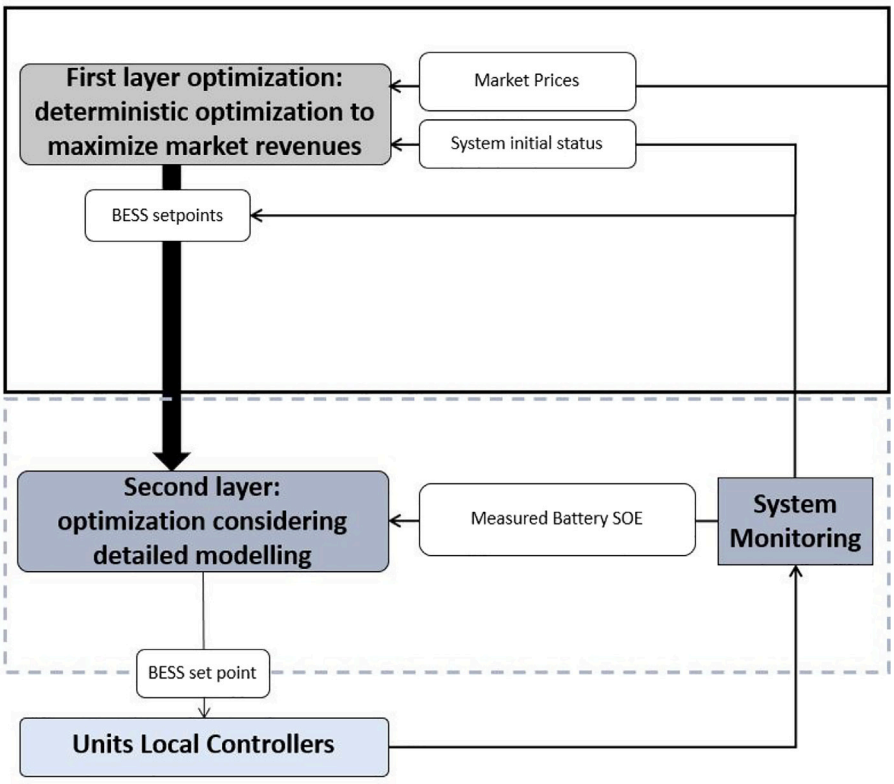

Fig. 3. Proposed two-level model scheme.

3.1.1. Cumulative degradation function and stress factors

In (11a), d_t^{op} includes d_t^{time}; since the latter is comparatively less than the product, it can be neglected. Also, temperature stress factor is neglected considering an efficient cooling system implemented.

In (11a) there is a product of three continuous variables $d_t^{CR} d_t^{DoD} d_t^{SoE}$, which is difficult to be handled in a linear model; in particular, there is not a clear way to multiply more than two continuous variables in a linearized fashion. Therefore, a worst-case scenario has been taken for the value of DoDs, considering the highest DoD and using it to calculate f^{DoD} through (20). This approximation can overestimate the stress factor, being on the safe side for evaluating degradation:

$$\tilde{\overline{d}}^{DoD}(\tilde{\overline{DoD}}) = \frac{1}{\tilde{K}^{\delta_1}\tilde{\overline{DoD}}^{\tilde{K}^{\delta_2}} + \tilde{K}^{\delta_3}} \tag{39}$$

The linearized stress factors are now used for the formulation of a cumulative degradation function in real-time, expressed as:

$$d_t^{op} = d_t^{SoE}\, d_t^{CR}\, \tilde{\overline{d}}^{DoD}(\tilde{\overline{DoD}}) \tag{40}$$

The product of d_t^{SoE} and d_t^{CR}, two continuous variables, can be convexified using the techniques described in [54] as:

$$N = QM = \left(\frac{Q+M}{2}\right)^2 - \left(\frac{Q-M}{2}\right)^2 \tag{41}$$

where Q, M are two generic continuous variables.

Therefore:

$$d_t^{SoE}\, d_t^{CR} = SQ_t^{d^{SoE}, d^{CR}} - DQ_t^{d^{SoE}, d^{CR}} \tag{42}$$

Following similar considerations, in (11b) the temperature stress factor can be neglected; moreover, once defined Δt, also d_t^{time} becomes constant and can be threaded as a parameter. Therefore, (11b) becomes:

$$d_t^{id} = \tilde{d}_t^{time} \tilde{d}_t^{Temp} d_t^{SoE} \tag{43}$$

thus becoming only SoE-dependent.

Finally, due to the convexity of the exponential function, (15) and (19) can be linearized through piecewise linearization [55].

In (12), there are the products $d_t^{op} Z_t^{op}$ and $d_t^{id} Z_t^{id}$, that represents the multiplication between a continuous variable and a binary one. Let Z be a binary variable and Q a continuous one for which $Q \le \tilde{U}$, where $\tilde{U}$ is the upper bound of Q; a continuous variable Y is introduced to replace the product $Y = QZ$. The linearization can be achieved through the following additional constraints [54]:

$$Y \le \tilde{U} Z \tag{44a}$$

$$Y \le Q \tag{44b}$$

$$Y \ge Q - \tilde{U}(1 - Z) \tag{44c}$$

Therefore, (12) can be split into two set of equations without using any auxiliary binary variable:

$$d_t \le \tilde{\overline{d}}^{op} Z_t^{op} \tag{45a}$$

$$d_t \le \tilde{\overline{d}}^{op} \tag{45b}$$

$$d_t \ge d_t^{op} - (1 - Z_t^{op})\tilde{\overline{d}}^{op} \tag{45c}$$

and:

$$d_t \le \tilde{\overline{d}}^{id} Z_t^{id} \tag{46a}$$

$$d_t \le \tilde{\overline{d}}^{id} \tag{46b}$$

$$d_t \ge d_t^{id} - (1 - Z_t^{id})\tilde{\overline{d}}^{id} \tag{46c}$$

3.1.2. Life loss

Battery remaining life and life loss at the time instance t are given by (9) and (14) respectively. Exponents in (9) are relatively small when considering time periods typical for operation (several hours). For longer study periods, the use of rolling time horizon allows optimization over short periods of time. Hence, in general for short time periods, $\tilde{\beta} \in [10^1; 2 \cdot 10^2]$, while $d_t \in [10^{-8}; 8 \cdot 10^{-5}]$ [21,22]. Therefore,

$\tilde{\beta} \cdot d_t$ is, in the worst case, 10^{-2}. Moreover, for old batteries, since the SEI film formation stops and the battery degrades slower, $\tilde{\alpha}$ becomes zero and $\tilde{\beta} \cdot d_t$ term disappears from (9). It is possible then to exploit the linear approximation that a function $g(x) = e^{f(x)}$, with $f(x)$ close to zero, can be expressed as $g(x) = 1 + f(x)$. Therefore, (9) becomes,

$$BRL_t = \tilde{\alpha}(1 - \tilde{\beta} d_t) + (1 - \tilde{\alpha})(1 - d_t) \tag{47}$$

$$BRL_t = 1 - d_t[1 + \tilde{\alpha}(\tilde{\beta} - 1)] \tag{48}$$

Substituting (48) in (14), if the battery is new ($\tilde{L}^{init}$=100%), it becomes:

$$L_t = [1 + \tilde{\alpha}(\tilde{\beta} - 1)] d_t = \tilde{m}^{LL,new} d_t \tag{49}$$

This approximation is valid as long as the exponent remains sufficiently small; in normal applications, the simulation time intervals are not very large and linearization is acceptable.

For an old battery, $\tilde{\alpha}$ becomes zero [21]; hence, $\tilde{m}^{LL,old} = 1$ and (49) becomes:

$$L_t = d_t \tag{50}$$

Finally, L_t can be divided into operating life loss, L_t^{op}, and idle life loss, L_t^{id}, as follows:

$$L_t = L_t^{op} + L_t^{id} \tag{51}$$

$$L_t^{op} = \tilde{m}^{LL} d_t^{op} \tilde{n}_{cy} \tag{52}$$

$$L_t^{id} = \tilde{m}^{LL} d_t^{id} \tag{53}$$

3.2. Efficiencies

To avoid variables multiplication, efficiencies have been treated as losses within the component:

$$X\eta = X - Losses$$

$$\frac{Y}{\eta} = Y - Losses$$

where X is a generic positive number and Y is a generic negative one.

3.2.1. Battery

The internal resistance of the electrodes and the electrolytes of Li-ion batteries increases gradually due to repeated cycling [56,57]. Losses associated with the resistance can be expressed as:

$$P^{loss,bat} = R^{bat} I^2 \tag{54}$$

Current flowing through the battery is proportional to CR:

$$I = \frac{CR \cdot E}{V} \tag{55}$$

where E is the battery energy, V is the battery voltage level and CR is defined as in (7). Resistance values mainly depend on the battery SoE and SoH [48]. By (55), it is possible to rewrite (54) as:

$$P^{loss,bat} = R^{bat}(SoH, SoE) CR^2 \frac{E^2}{V^2} \tag{56}$$

The effects of SoH and SoE on the battery resistance has been split considering that SoH of each battery varies little within an optimization cycle and can be assumed as a parameter, $S\tilde{o}H^f$. Resistance is therefore only SoE-dependent and (56), considering E as a parameter through (32) and the voltage constant on the Direct Current (DC) side of the converter, becomes:

$$P_{s,t}^{loss,bat} = S\tilde{o}H_s^f R_{s,t}^{bat}(SoE) CR_{s,t}^2 \frac{\tilde{E}_s^2}{\tilde{V}_s^2} \tag{57}$$

Therefore, linearization of (57) is reduced to the linearization of the $R_{s,t}^{bat}(SoE) CR_{s,t}^2$ product.

Due to its convexity, $CR_{s,t}^2$ can be linearized using the CCV method.

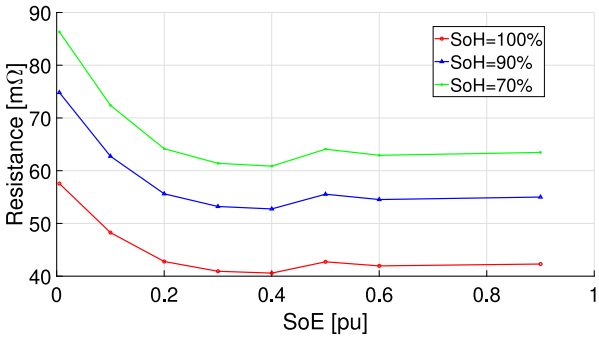

Fig. 4. Battery resistance value as function of SoE [58].

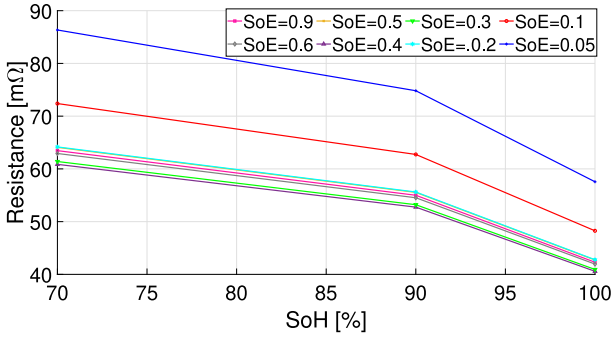

Fig. 5. Battery resistance value as function of SoH [58].

The $R^{bat}(SoE)$ term can be linearized starting from Fig. 4, where battery resistance values used in this study and typical for Li-ion batteries are plotted as a function of the SoE.

The SoE range can be divided into two subsets (0.05–0.5 and 0.5–0.9) and in each of them the resistance is a convex function:

$$R_{s,t}^{bat} = R_{s,t}^{bat,a} Z_{s,t}^a + R_{s,t}^{bat,b} Z_{s,t}^b \tag{58a}$$

$$SoE_{s,t} = SoE_{s,t}^a Z_{s,t}^a + SoE_{s,t}^b Z_{s,t}^b \tag{58b}$$

Eqs. (58) are used to select the two different subsets: for each time instant, only one between $Z_{s,t}^a$ and $Z_{s,t}^b$ is equal to 1 and only one part of the curve is considered. The two curves can be linearized separately by piecewise linearization through the CCV method. The products in (58) can be linearized as in [54].

Parameter $S\tilde{o}H^f$ can be calculated starting from Fig. 5, where the resistance values are plotted as a function of the SoH as follows:

To set $S\tilde{o}H^f$, the following steps have been followed:

1. for each given SoH (100%, 90%, 70%) the average value of the resistance over the SoE range has been calculated;
2. using curve fitting, linear approximation of $R(SoH)$ is obtained;
3. using it, the value of $S\tilde{o}H$ is obtained by $R(100\%)/R(SoH)$, where SoH is the actual value before optimization.

Lastly, the product $R_{s,t}^{bat} CR_{s,t}^2$ can be linearized as described in [54] and explained earlier in (41):

$$R_{s,t}^{bat} CR_{s,t}^2 = SQ_{s,t}^{R^{bat},CR^2} - DQ_{s,t}^{R^{bat},CR^2} \tag{59}$$

with both terms modeled through piecewise linearization.

Hence, (2), suitably adapted for a system of several batteries and considering variable efficiency, becomes:

$$SoE_{s,t} = SoE_{s,t-1} + \frac{\tilde{\Delta t}}{\tilde{E}_s}(P_{s,t}^{chg} + P_{s,t}^{dis} - P_{s,t}^{loss,bat}) \tag{60}$$

where $P_{s,t}^{loss,bat}$ linearization is given by (57)–(59).

Table 1
First level battery data.

$\tilde{SoE}^{init}$ [pu]	$\tilde{L}^{init}$ [%]	$\tilde{CR}$ [h^{-1}]	$\tilde{\bar{E}}$ [MWh]	$\tilde{\bar{P}}^{chg}$ [MW]	$\tilde{\bar{P}}^{dis}$ [MW]	$\tilde{\eta}$ [%]
0.5	95.62	1	6.88	7.2	−7.2	96.5

3.2.2. Converter

Converters losses can be classified as: conduction losses, off-state losses and switching losses. Since the leakage current during the off-state of the device is negligibly small, power losses during the off-state can be neglected [59]. Conduction losses are dependent on the square value of the current, whereas the switching ones depend on the current and the switching frequency [60], which is constant. In general, also the voltage at the DC bus and the modulation index have effects on the losses; since the DC voltage has small variations with the SoE, these last contributions can be neglected, resulting in an error lower than 0.2% [61].

Therefore, semiconductor losses can be modeled as:

$$P_{s,t}^{loss,conv} = \tilde{\gamma}_{s,t} I_{s,t}^{conv^2} + \tilde{\zeta}_{s,t} I_{s,t}^{conv} + \tilde{\lambda}_{s,t} \tag{61}$$

where $\tilde{\gamma}_{s,t}, \tilde{\zeta}_{s,t}, \tilde{\lambda}_{s,t}$ are parameters that can be evaluated through experimental data; in particular, $\tilde{\lambda}_{s,t}$ represents no-load losses. Since the DC voltage can be assumed constant and current is proportional to the apparent power through the converter, (61) becomes:

$$P_{s,t}^{loss,conv} = \tilde{\gamma'}_{s,t} A_{s,t}^{conv^2} + \tilde{\zeta'}_{s,t} A_{s,t}^{conv} + \tilde{\lambda'}_{s,t} \tag{62}$$

The term $A_{s,t}^{conv^2}$ can be expressed as:

$$A_{s,t}^{conv^2} = P_{s,t}^{conv^2} + Q_{s,t}^{conv^2} = \\ = (P_{s,t}^{chg,conv} - P_{s,t}^{dis,conv})^2 + Q_{s,t}^{conv^2} \tag{63}$$

Due to their convexity, variables $P_{s,t}^{conv^2}$ and $Q_{s,t}^{conv^2}$ are linearized through the CCV method mentioned above. Therefore, it is possible to linearize the convex term of $P_{s,t}^{loss,conv}$ in (62) through the CCV method, since it depends on the sum of two convex functions [62].

Eqs. (8a) and (8b), adapted for a system of several batteries and considering variable efficiency, become:

$$P_{s,t}^{chg} = P_{s,t}^{chg,conv} - P_{s,t}^{loss,conv} Z_{s,t}^{chg} \tag{64a}$$

$$P_{s,t}^{dis} = P_{s,t}^{dis,conv} - P_{s,t}^{loss,conv} Z_{s,t}^{dis} \tag{64b}$$

The products $P_{s,t}^{chg,conv} Z_{s,t}^{chg}$ and $P_{s,t}^{dis,conv} Z_{s,t}^{dis}$ are linearized through the techniques described in [54] and illustrated by (44).

3.2.3. Transformer

Transformers losses have been modeled starting from the Cantilever equivalent circuit, in which the shunt branch is moved to the primary terminals [63]. Eqs. (37) become:

$$P_{c,t}^{trans,prim} = P_{c,t}^{trans,sec} + \tilde{P}_c^{fe} + P_{c,t}^{joule,tr} = \\ = P_{c,t}^{trans,sec} + \tilde{P}_c^{fe} + 3\tilde{R}_c^{s,tr} I_{c,t}^{sec'^2} \tag{65a}$$

$$Q_{c,t}^{trans,prim} = Q_{c,t}^{trans,sec} + \tilde{Q}_c^{hyst} + Q_{c,t}^{flux,tr} = \\ = Q_{c,t}^{trans,sec} + \tilde{Q}_c^{hyst} + 3\tilde{X}_c^{s,tr} I_{c,t}^{sec'^2} \tag{65b}$$

The term $I_{c,t}^{sec'^2}$ can be expressed as:

$$I_{c,t}^{sec'^2} = \frac{P_{c,t}^{trans,prim^2} + Q_{c,t}^{trans,prim^2}}{3V^{n,sec^2}} \tag{66}$$

where terms $P_{c,t}^{trans,prim^2}$ and $Q_{c,t}^{trans,prim^2}$ are linearized through CCV method.

3.2.4. Convexity and objective function

Adding the losses in the objective function allows the exploitation of the CCV method. Therefore, (33) becomes:

$$Min\ \tilde{\Delta t} \sum_t (D_t^{obj} + L_t^{tot}) \tag{67}$$

with:

$$L_t^{tot} = \sum_s (P_{s,t}^{loss,bat} + P_{s,t}^{loss,conv}) + \tag{68}$$

$$+ \sum_c (P_{c,t}^{joule,tr} + Q_{c,t}^{flux,tr}) \tag{69}$$

Moreover, due to the minimization of the terms D_t^{obj} and $P_{s,t}^{loss,bat}$, the subtracted terms of the linearization of the product of variables in (42), $DQ_t^{d^{SoE},d^{CR}}$, and (59), $DQ_{s,t}^{R^{bat},CR^2}$, have to be included as penalty factors, since the optimization problem, in an attempt to minimize the terms, will maximize the variable to be subtracted. Therefore:

$$f_t^{pen} = \sum_s (CR_{s,t}^2 + DQ_{s,t}^{d^{SoE},d^{CR}} + DQ_{s,t}^{R^{bat},CR^2}) \tag{70}$$

and (67) becomes:

$$Min\ \tilde{\Delta t} \sum_t (D_t^{obj} + L_t^{tot} + f_t^{pen}) \tag{71}$$

Therefore, the first level optimization linearized model is made of: OF : (27) $s.t.$: (2)–(8), (13)–(15), (19)–(21), (24)–(26), (28)–(32), (39)–(46), (48), (51)–(53). while the second level optimization linearized model is made of:

OF : (71)

$s.t.$: (3)–(8), (13)–(15), (19)–(21), (32), (36), (38)–(46), (48), (51)–(53), (57)–(60), (62)–(66), (68), (70).

4. Results

4.1. Input data

Concerning the first level, ratings and battery constraints as provided by the manufacturer are shown in Table 1.

Parameter $\tilde{N}^{cy}$ has been set equal to 3. To calculate the operating cost of the BESS, monetary values have been taken from [7] and an overall cost of 310 $\frac{€}{kWh}$ has been considered. Parameters η^{conv} and η^{trans} have been assumed equal to 98% and 99%, respectively [58].

Market data, taken from [64], are referred to Italy North bidding zone (May 2020), with parameter Δt^{BSP} chosen between 17:00 and 20:00.

Considering the second level, a system made of five batteries, each equipped with their own converter and connected with two identical groups of transformers, has been considered; their data are summarized in Table 2. Bat1, Bat2, and Bat3 are connected to the first transformer, while Bat4 and Bat5 are connected to the second one.

Transformer data [58] is summarized in Table 3.

The reactive power profile has been defined by setting a random value between −0.72 Mvar and +0.72 Mvar, which is the 8% of the nominal plant size; this choice was made considering BESS operation close to unitary power factor, as no reactive power services have been imposed to the plant.

The MILP optimization problem has been implemented in GAMS 32.2.0 and solved using CPLEX 12.6. Simulations have been performed on a PC with Intel®Core™i7-3770 CPU @ 3.40 GHz, RAM 8 GB.

Table 2
Second level battery data [58].

	$\tilde{L}^{init}$ [%]	$\tilde{\overline{E}}$ [MWh]	$\tilde{SoH}^{f}$ [–]	$\tilde{SoE}^{init}$ [pu]	$\tilde{\underline{SoE}}$ [pu]	$\tilde{\overline{SoE}}$ [pu]	$\tilde{\overline{CR}}$ [h^{-1}]	$\tilde{\overline{P}}^{chg}$ [MW]	$\tilde{\underline{P}}^{dis}$ [MW]
Bat1	100	1.8	1.0	0.5	0.1	0.9	1	1.8	−1.8
Bat2	93	1.674	1.21	0.5	0.1	0.9	1	1.8	−1.8
Bat3	99	1.782	1.03	0.5	0.1	0.9	1	1.8	−1.8
Bat4	96	1.728	1.12	0.5	0.1	0.9	1	1.8	−1.8
Bat5	90.1	1.622	1.297	0.5	0.1	0.9	1	1.8	−1.8

Table 3
Transformer parameters [58].

$\tilde{A}^{n}$ [MVA]	$\tilde{V}^{n,p}$ [kV]	$\tilde{V}^{n,s}$ [kV]	$\tilde{v}^{cc}$ [%]	$\tilde{P}^{cc}$ [kW]	$\tilde{P}^{fe}$ [kW]	$\tilde{i}^{0}$ [%]
5.4	36	0.4	6	32	4.3	0.13

4.2. Model effectiveness evaluation

4.2.1. Short-term analysis

To verify the effectiveness of the model, the three strategies introduced in 2.2 have been simulated over 31 days (744 h). For each day, the first level sets a profitable real power load profile considering the entire day; once defined, the profile is given as input, together with the reactive power as described in 4.1, to the second level which splits the profiles between the single batteries within the BESS. The second level is simulated using the rolling horizon approach: the optimization was considered for intervals of three hours, with time step of one hour, using the rolling horizon along one day (the one simulated by the first level). For each three-hours interval, only the first one is considered applied in operation and then used as initial condition for the next rolling horizon iteration; in other words, the first hour is optimized while considering one hour before and two ahead.

Moreover, the sensitivity of the three strategies respect to $\tilde{\alpha}$ has been tested.

Considering the second level, Fig. 6 shows the values of cumulative $d_{s,t}$ and cumulative $L_{s,t}$ for Strategy A, that represents the current industrial practice, in which the system does not prioritize the use of any battery and loads them equally. This causes a significant capacity degradation which, as shown in Fig. 6(a), is similar for the five batteries; the capacity degradation is not exactly the same given the different $\tilde{SoH}^{init}$ which leads to a different value of Joule losses. Also Fig. 6(b) highlights the similar batteries behavior: Bat5 has the same trend as the others until the SoH value of 90% is reached. Beyond this point, the slope $\tilde{m}^{LL}$ from (52)–(53) changes and Bat5 loses less life than the others, despite similar degradation values.

In Strategy B, the second level minimizes $\frac{d_{s,t}}{\tilde{L}_s^{init}}$, thus considering only $\tilde{L}_s^{init}$, since $\tilde{\alpha}$ and $\tilde{\beta}$ do not influence directly $d_{s,t}$. The values of cumulative $d_{s,t}$ and cumulative $L_{s,t}$ are shown in Fig. 7. Strategy B simulates the priority of using newer batteries more, without considering the change of slope of the $L_{s,t}$ curve due to the zeroing of $\tilde{\alpha}$, to balance their SoH. Fig. 7(a) shows that Bat1, the newest, is the one that degrades the most, followed by Bat3, Bat4, Bat2 and lastly Bat5, according to their age (Table 2); a similar behavior is observed in Fig. 7(b).

In Strategy C, the second optimization level minimizes $\frac{L_{s,t}}{\tilde{L}_s^{init}}$, thus considering both $\tilde{L}_s^{init}$ and $\tilde{\alpha}$ which, as described in Section 3.1.2, influence $L_{s,t}$ as it becomes 0 once the battery reaches a SoH lower than 90%. Considering the second level, the values of cumulative $d_{s,t}$ and cumulative $L_{s,t}$ are shown in Fig. 8: Strategy C simulates the priority of using newer batteries more, but also considering the change of slope of $L_{s,t}$ curve due to the zeroing of $\tilde{\alpha}$. Fig. 8(a) shows that Bat1, the newest, is the one that degrades the most. However, compared to Strategy B, Bat5, the oldest, has a higher cumulative degradation due to the change in slope of $\tilde{m}^{LL}$ from (52)–(53) which, for equal $d_{s,t}$, leads to a lower value of $L_{s,t}$. Therefore, the smaller value of the numerator of $\frac{L_{s,t}}{\tilde{L}_s^{init}}$ influences the objective function more than the smaller value of the denominator which, as previously mentioned, would penalize the use of older batteries. In Fig. 8(a), Bat5 curve changes slope at h = 308 and crosses the curves of Bat2, Bat4 and Bat3 at h = 478, h = 631 and h = 735, respectively. Up to h = 308, curves in Fig. 7(a) and 8(a) are the same, as the strategy until $BRL_{s,t}$ = 90% is the same. Considering Fig. 8(b), even if Bat5 is more used than Bat2, Bat3 and Bat4, it has a lower cumulative $L_{s,t}$, because of the zeroing of $\tilde{\alpha}$. As a result, Bat2, the second oldest after Bat5, will be used less; this behavior determines the almost horizontality of its curves in Fig. 8(a) and 8(b).

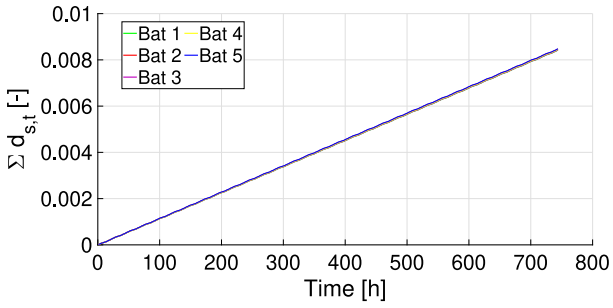

(a) Cumulative $d_{s,t}$

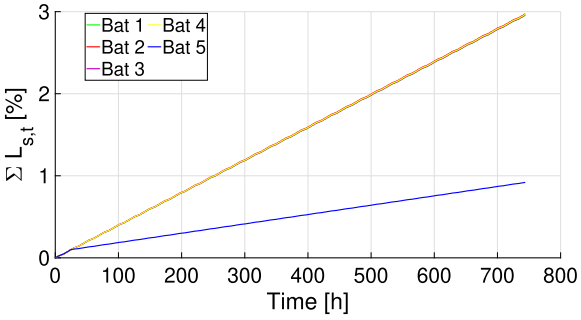

(b) Cumulative $L_{s,t}$

Fig. 6. Strategy A: degradation results.

Table 4 synthesizes the results of optimization at both levels. Simulation times indicated in column "t^{sim}" are very short for Strategy A, while they are longer for the other two, although they remain contained.

According to Table 4, Strategy A gives the worst results both from the point of view of profits and life loss. Between Strategies B and C differences are small: life loss in Strategy C is 0.946% smaller than in Strategy B (last column), which is about 0.2% per battery, but profits are 90 € lower (second column), which is around 0.33% of total. For longer periods, the difference in life loss can become significant, leading to more battery replacements. However, the simulation interval of one month is too short for an in-depth comparison between Strategies B and C, and is performed in the vicinity of average battery remaining life of ≈ 90%, testing the adopted strategies against SEI film formation stop, when $\tilde{\alpha}$ becomes null; therefore, in Section 4.2.2 a wider time interval is analyzed.

Table 4
Simulation results.

	t^{sim}	First level			Second level			
		$\sum_t Pr_t$	$\sum_t R_t$	$\sum_t C_t^d$	$\sum_{s,t} P_{s,t}^{loss,bat}$	$\sum_{s,t} P_{s,t}^{loss,conv}$	$\sum_{s,t} d_{s,t}$	$\sum_{s,t} L_{s,t}$
	[h:min:s]	[€]	[€]	[€]	[MWh]	[MWh]	[–]	[%]
Strategy A	0:10:18	27150	53020	25870	9.721	34.477	0.0413	12.655
Strategy B	1:43:27	27640	53420	25780	24.449	20.42	0.0209	7.254
Strategy C	1:07:56	27550	53270	25720	24.820	20.39	0.0212	6.308

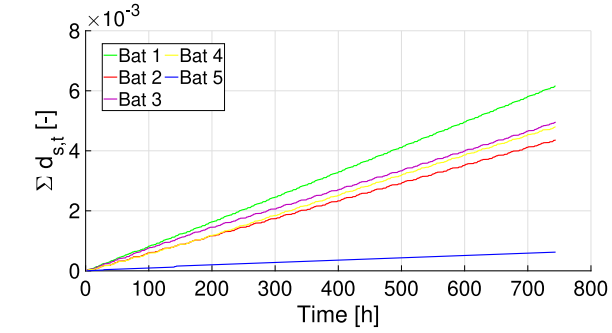

(a) Cumulative $d_{s,t}$

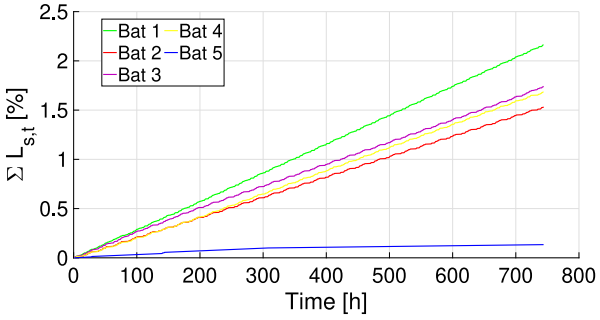

(b) Cumulative $L_{s,t}$

Fig. 7. Strategy B: degradation results.

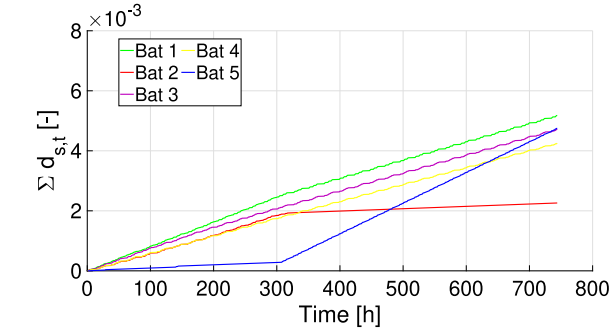

(a) Cumulative $d_{s,t}$

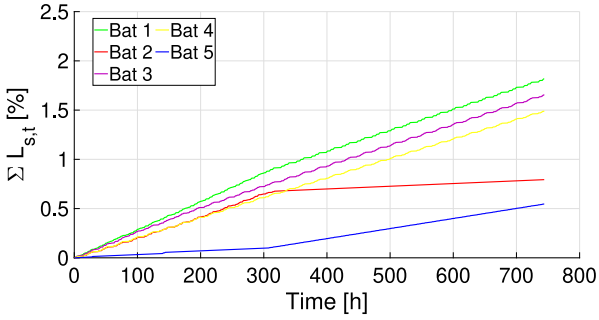

(b) Cumulative $L_{s,t}$

Fig. 8. Strategy C: degradation results.

The different values in the "First level" columns in Table 4 depends on the strategy adopted: even if, as stated in the Introduction, the two levels are independent, the maximum bids that the BESS can submit vary as a function of the remained capacity, which depends on the second level results of previous periods computations.

4.2.2. Long-term analysis

The long-term impact of the three strategies considered is analyzed through a 10-year simulation. Being interested primarily in the results of the second level and being very difficult to estimate prior evolution in log term for ASM and BM, the parameters related to the ASM and BM in the first optimization level are considered constant, and equal to the ones used for short-term analysis, throughout the analyzed period.

Fig. 9, 10, and 11 show the remaining life for each of the five batteries considered; here a battery is replaced when it reaches $BRL_{s,t} = 80\%$.

While for Strategy A the behavior is similar to that described in 4.2.1, the same cannot be said for Strategies B and C. A clear example is represented around the fifth year: in Strategy B (Fig. 10), Bat2 waits a long time before being replaced (almost a year), while in Strategy C (Fig. 11) everything happens much more quickly. This difference derives from the different numerator between the two strategies; in fact, that of Strategy B is independent of $\tilde{\alpha}$ and therefore the numerator for an old battery is much stronger than a new battery one, leading, as expected, to less use of old batteries compared to new ones (the remaining old battery is significantly slowed down once Bat2 is replaced). On the other hand, in Strategy C the effect of the numerator also depends on $\tilde{\alpha}$, which leads to a more uniform behavior between batteries with different levels of BRL.

Table 5 summarizes the total number of replacements year by year; it can be easily observed that the substitutions in Strategy A are much higher than those in the other two, confirming the greater efficiency of the new proposed strategies compared to the traditional one. Moreover, the profits with Strategy A are around 2.6924 $M€$, a lower value than the other two strategies, which are 3.3588 $M€$for Strategy B and 3.4696 $M€$for Strategy C. In the decade studied (2020/2030), Strategy B replaces slightly less batteries than Strategy C and the amount of money saved by using Strategy B over Strategy C is around 217.25 $k€$; this value considers that only 20% of the whole capacity will be refilled and that cost of the BESS is assumed to decrease along the years as for [7]. On the other hand, the difference in profits is 110.8 $k€$ between the two strategies in favor of Strategy B. These results show that Strategy B would seem to be of slighter better efficiency in monetary terms than Strategy C, since the money saved by the lower number of replacements is greater than that not earned in terms of profits. However, using Strategy B instead of C allows for fewer substitutions, but more distributed over time; this latter effect must be considered by the owner of the BESS, as it could results in a greater number of plant maintenance periods, thus higher time with resources unavailable.

However, these conclusions highly depend on the starting price of the BESS, on the initial remaining life of BESS batteries at the start of

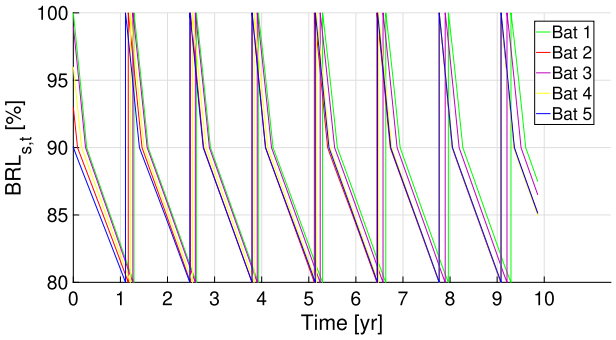

Fig. 9. Strategy A: 10 years simulation.

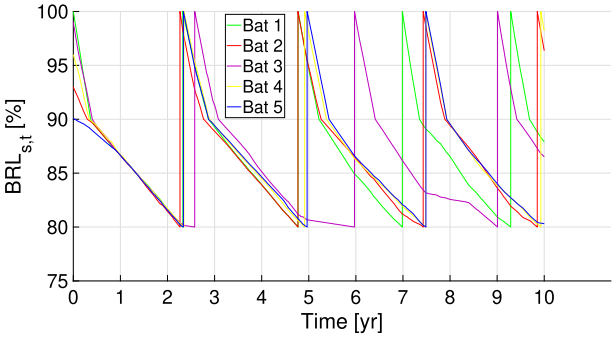

Fig. 10. Strategy B: 10 years simulation.

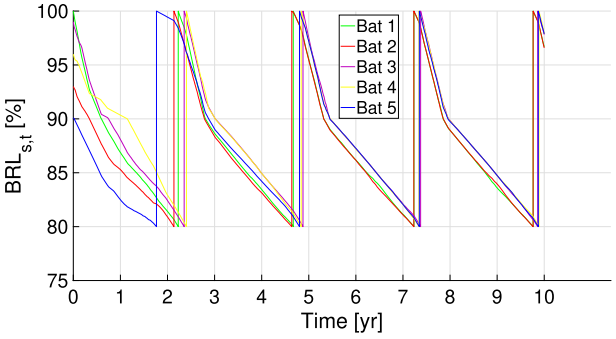

Fig. 11. Strategy C: 10 years simulation.

Table 5
Long-term analysis: Number of battery replacements for each strategy.

	Year											Tot.
	0	1	2	3	4	5	6	7	8	9	10	
A	0	5	5	5	0	5	5	5	0	5	0	35
B	0	0	5	0	4	1	1	2	1	3	0	17
C	0	1	4	0	5	0	0	5	0	5	0	20

the long-term evaluation (as it influences the nominators of the objective function, hence the relative importance given to each battery), and on the prices in the electricity market; the latter are difficult to predict, and therefore cannot be commented upon. On the other hand, the BESS replacement cost reduction can be more reliable [7]; therefore, for the considered plant configuration and starting data, and assuming invariant ASM prices over time, replacement costs in the remaining eight decades of the 21st century were compared to see their trend with respect to lost profits. Fig. 12 shows the results: with the data used in the study, it is noted that Strategy C will lead to better benefits than Strategy B starting from the fifth decade (2040/2050), i.e. when

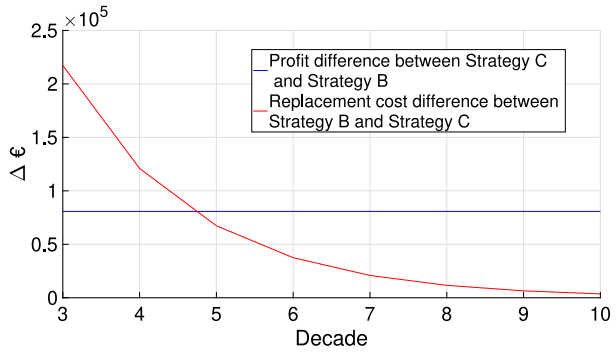

Fig. 12. Long-term analysis: comparison over the 21st century decades of the difference between profits and replacement costs.

the price of the batteries could be sufficiently lower to allow a greater number of replacements to be able to offer more power (resulting in higher profits).

Clearly, this result is dependent on the external assumptions: a different evaluation of ASM in time or a different plant configuration could lead to Strategy C becoming more advantageous earlier. In any case, it is clear that the paper proposes a useful tool not only for real-time optimal operation of BESS, but also for long-term analysis and, therefore, planning of a BESS plant and investments.

4.3. Mathematical model validation

To validate the model from a formal point of view, the impact of the relevant proposed linearizations and the scalability are analyzed; for the sake of illustration, Strategy C has been chosen for the analysis. Same qualitative results can be obtained also for Strategies A and B.

4.3.1. Linearization accuracy and impact

First, the accuracy of the linearization of the products $d^{SoE} \cdot d^{CR}$ from (40) and (42), and $R^{bat} \cdot CR^2$ from (57) and (59), together with the linear approximation of e^{-d_t} from (47), (48), and (49) have been considered. Table 6 shows the errors between different linearization techniques and real values obtained considering the entire range of possible values of the multiplied variables. For the two linearized products, the first line represents the actual product of the linearized variables, the second line represents the linearized product of the linearized variables, whereas, in the third one, one of the variables is fixed at average value, which is in line with approaches found in literature [28–30,34,35], where at most only one of the factors is considered dependent on operating conditions, while the remaining are assumed constant. Clearly, the proposed approach gives more accurate results. In particular, the approximation of the exponential function has very low relative percentage errors.

Second, a comparison between the most common optimization model found in literature, with degradation dependent only on SoE and constant efficiencies of the components [28], and the proposed model has been carried out. Converters and transformers efficiencies have been set as in Section 4, whereas battery efficiency and d^{CR} have been set equal to 98.03% and 0.94 respectively, which represent their average values. At the end of the optimization, the values of the power set-points obtained have been applied to the complete, non-linear physical model of batteries using MATLAB, to simulate the actual operation and, therefore, understand the impact of the approximations on actual operation. Results are summarized in Tables 7 and 8, with Strategy C applied. The proposed model better approximates the real physical model than the basic model, as for battery capacity degradation and SoE; in particular, in the proposed model, the maximum percentage relative error is 0.082% for BRL, 2.83% for degradation, and 0.58% for SoE, which are very reasonable and at least an order of magnitude

Table 6
Linearization errors.

	$d^{SoE}d^{CR}$	
	$\epsilon_{r,\%}^{max}$	$\epsilon_{r,\%}^{avg}$
Real prod. of Lin. var.	0.54	0.35
Lin prod. of Lin. var.[a]	2.35	0.41
Real prod. of Lin. $d^{SoE}\&d^{CR,avg}$ [28]	64.54	27.45
	$R^{bat}CR^2$	
	$\epsilon_{r,\%}^{max}$	$\epsilon_{r,\%}^{avg}$
Real prod. of Lin. var.	15.42	2.82
Lin prod. of Lin. var.[a]	19.55	2.97
Real prod. of Lin. $CR^2\&R^{bat,avg}$ [35]	21.84	5.23
	e^{-d_i}	
	$\epsilon_{r,\%}^{max}$	$\epsilon_{r,\%}^{avg}$
Lin. approx. $e^{f(x)} \approx 1 + f(x)$[a]	5.96 10^{-5}	1.35 10^{-5}

[a]Proposed model.

Table 7
Strategy C: Basic model errors.

	BRL [%]			d [–]	SoE [pu]
	GAMS	Real[a]	$\epsilon_{r,\%}$	$\epsilon_{r,\%}^{avg}$	$\epsilon_{r,\%}^{avg}$
Bat1	97.23	97.52	−0.30	30.51	52.76
Bat2	91.63	91.24	0.43	9.91	24.34
Bat3	97.45	97.25	0.21	11.71	14.62
Bat4	95.45	95.34	0.11	2.67	2.14
Bat5	89.33	89.39	−0.063	24.97	18.87

[a]Maximum DoD considered.

Table 8
Strategy C: Proposed model errors.

	BRL [%]			d [–]	SoE [pu]
	GAMS	Real[a]	$\epsilon_{r,\%}$	$\epsilon_{r,\%}^{avg}$	$\epsilon_{r,\%}^{avg}$
Bat1	98.18	98.10	0.082	1.96	0.40
Bat2	92.21	92.15	0.065	1.09	0.49
Bat3	97.34	97.28	0.062	1.38	0.58
Bat4	94.51	94.48	0.032	1.65	0.20
Bat5	89.55	89.53	0.022	2.83	0.38

[a]Maximum DoD considered.

smaller than their basic model counterparts, where the degradation and SoE errors are unacceptably high.

To be noted, since in this study a constant DoD has been considered, the values in the 'Real' columns have been obtained using the maximum DoD and the correspondent stress-factor, as the goal of this stage was to analyze the impact of the linearized product of variables.

A further comparison was made on the values of Over Operating Limits Violation (OOLV), defined as the number of hours in which the real physical model SoE exceeds the maximum or minimum limits imposed in the optimization constraints (i.e., 0.1 and 0.9 pu, respectively). These values are of particular importance because they establish for how many periods of time the batteries in the BESS are used more than what was foreseen by the optimization study, thus increasing their actual degradation. The amount of OOLV for each battery and for both the basic and proposed models are shown in Fig. 13, for various levels of SoE magnitude violations. For batteries from 1 to 4, the number of violations is lower for the proposed model than for the basic one, while for Bat5 the opposite occurs, but low values are found in both cases. On the other hand, the magnitude of violations in the proposed model is negligible, while in the basic model they are significant and can result in unexpected high levels of additional degradation. Hence, this confirms the far better accuracy of proposed model, which guarantees an optimal reliability of the operation of BESS.

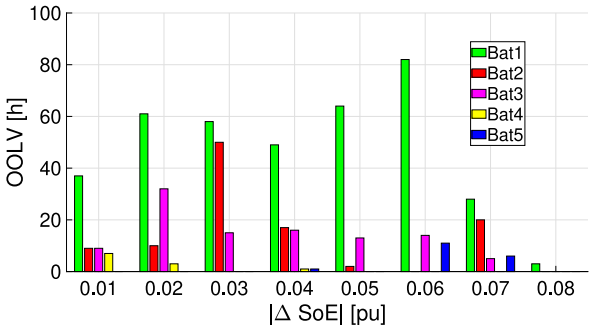

(a) Basic model

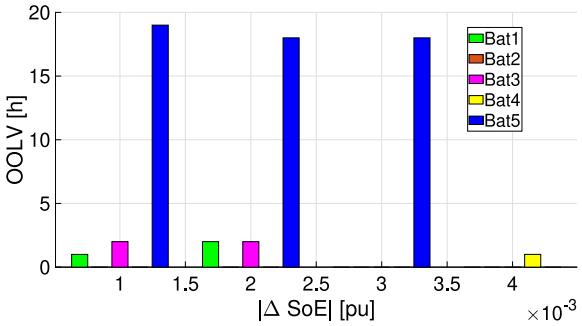

(b) Proposed model

Fig. 13. Strategy C: number of OOLV for different SoE magnitudes violations.

Table 9
Strategy C: Comparison between different levels of modeling for 31-days simulation.

	t^{sim} [h:min:s]	$\sum_t Pr_t$ [k€]	$B\tilde{R}L^{av}$ [%]
Basic model	0:09:23	27.78	93.9659
Mod2	0:14:05	27.80	93.9612
Mod3	0:16:18	27.79	94.0098
Mod4	0:34:59	27.55	94.0353
Proposed model	1:07:56	27.55	94.1629

Table 10
Scalability of the proposed model: One day simulation.

# Bat –	# Var –	# Bin –	t^{sim} [h:min:s]	$t^{sim,av}$ [min:s]	$\tilde{t}^{sim}$ [min:s]
5	7321	1560	0:04:01	00:10	00:28
6	8665	1872	0:11:33	00:29	01:01
7	10009	2184	0:20:56	00:52	02:07
8	11377	2496	0:50:39	02:07	05:24
9	12721	2808	2:03:39	05:09	10:33
10	14065	3120	4:27:35	11:09	36:01

Finally, an analysis of different levels of approximations has been carried out, starting from the basic model described earlier, and gradually adding more level of detail. The intermediate models considered are:

(i) **Mod2**, with constant efficiency and complete degradation, average value of battery internal resistance equal to 43.45 mΩ;
(ii) **Mod3**, with battery efficiency CR-dependent and complete degradation, average value of battery internal resistance equal to 43.45 mΩ;
(iii) **Mod4**, with battery efficiency as a function of SoE and CR and complete degradation.

Strategy C optimization results are shown in Table 9. Simulation time increases with the complexity of the model whereas remaining acceptable. Moreover, BRL value remains about the same with the basic model for all the intermediate models, while the profit gets to the same level with the proposed model only for Mod4. Even if the differences may seem small, the cumulative effect over long-term periods can be significant and can result in a higher risk of additional degradation and important financial losses. Clearly, the proposed model brings on important quality jump in modeling of BESS in optimization problems.

4.3.2. Scalability

The scalability of the model is checked. Clearly, as explained in the theoretical part, the first optimization level is not an issue as it uses simplified models to represent the BESS system in its whole and, in case of multiple BESS plants, decomposition techniques can be applied. Hence, the focus here is on the second level, where the batteries within a BESS are represented in detail, hence requiring many variables: for the sake of illustration, Strategy C has been considered. The number of batteries in the BESS system was increased from 5 batteries by adding one battery at a time and simulations over initial one-month period carried. Results are summarized in Table 10 for a BESS made of up to 10 independent batteries. As the number of batteries increases, the calculation times get longer, given the greater number of variables (columns "# Var" and "# Bin", the last one indicates the number of binaries). Considering an hour-by-hour calculation of the operation of BESS, for the 10 batteries case the average time (column "$t^{sim,av}$") is 11 min, while the maximum time (column "$\bar{t}^{sim}$") is 36 min, which is well within one hour. For BESS made of more than 10 batteries the computation time increases and becomes less compatible with real-time operations. However, for these cases, it is reasonable to assume the clustering of similar batteries to reduce the number of control variables and guarantee acceptable computation times.

The authors are aware that results in this Subsection in particular are influenced by computing resources, and that the limit if 10 batteries can be overcome with a better machine.

5. Conclusions

In this work, a new hierarchical two-level MILP optimization model for BESS operation has been implemented. In the first level, objective function is profit maximization, that comes from the trade-off between the revenues and costs in the participation in the ancillary service electricity market and the degradation cost of the batteries. In the second level the optimal load profile defined through the first level is distributed among the single batteries that make up the BESS; here, an advanced and linear battery degradation model has been developed that considers SoE, CR, time, and DoD as factors, together with SEI film formation, operating characteristics of batteries, converters, and transformers. Moreover, also three different EMS strategies have been implemented and their effect on the use of the single batteries has been studied.

The model has been tested using a realistic size BESS plant over a 31-days rolling horizon optimization and a 10-years one; the short-term analysis was made to verify the impact of the SEI formation on the priority use between new and old batteries, while the long-term one was aimed at studying its impact following battery replacements. Results show that, depending on the chosen strategy, it is possible either to maximize profits at a high degradation and life loss, or obtain improved life loss of batteries for a marginal decrease of profits.

Lastly, the impact of the complete model against others, more simple and in-line with literature models, has been evaluated: the accuracy of the linearizations and the results show very good performances of the proposed one.

CRediT authorship contribution statement

Riccardo Nebuloni: Conceptualization, Methodology, Software, Writing – original draft. **Lorenzo Meraldi:** Conceptualization, Resources, Validation. **Cristian Bovo:** Writing – review & editing, Visualization. **Valentin Ilea:** Conceptualization, Writing – review & editing. **Alberto Berizzi:** Supervision, Writing – review & editing. **Snigdh Sinha:** Writing – original draft, Formal analysis. **Raviteja Bharadwaj Tamirisakandala:** Writing – original draft, Formal analysis. **Pietro Raboni:** Resources, Writing – review & editing.

Declaration of competing interest

The authors declare that they have no known competing financial interests or personal relationships that could have appeared to influence the work reported in this paper.

Data availability

The authors do not have permission to share data.

Acknowledgments

This work was partly financed by NHOA, formerly ENGIE-EPS, in the framework of PROPHET Project. The authors thank NHOA for the technical contribution and access to the data-sheets.

Fundings

This research did not receive any specific grant from funding agencies in the public, commercial, or not-for-profit sectors.

Appendix

In this Appendix, constraints (25) are explained in detail. Suppose $\tilde{N}^{int} = 2$, which means that in the two-hours period two time intervals are present; moreover, a parameter $\tilde{t}^{acc}$, that is the time instant from which one begins to have accepted flexibility, is introduced. Let us consider, for example, constraint (25a), in which the apex "chg, PoC, ASM" is substituted with "X" for simplicity; for each P_t^X with $t < \tilde{t}^{acc}$, we have that $P_t^X \geq 0$. At $t = \tilde{t}^{acc}$ we have that $P_t^X \geq P^{acc}$, where P^{acc} is the accepted flexibility quantity; it follows that:

$$P_t^X \geq \begin{cases} P^X_{\tilde{t}^{acc}} - P^X_{\tilde{t}^{acc}-1} = P^{acc} \\ \qquad\qquad \text{if } t = \tilde{t}^{acc} + 1 \\ P^X_{\tilde{t}^{acc}-1} - P^X_{\tilde{t}^{acc}-1} = 0 \end{cases} \tag{A.1}$$

$$P_t^X \geq \begin{cases} P^X_{\tilde{t}^{acc}+1} - P^X_{\tilde{t}^{acc}} = 0 \\ \qquad\qquad \text{if } t = \tilde{t}^{acc} + 2 \\ P^X_{\tilde{t}^{acc}} - P^X_{\tilde{t}^{acc}} = 0 \end{cases} \tag{A.2}$$

$$P_t^X \geq \begin{cases} P^X_{\tilde{t}^{acc}+2} - P^X_{\tilde{t}^{acc}+1} = -P^{acc} \\ \qquad\qquad \text{if } t = \tilde{t}^{acc} + 3 \\ P^X_{\tilde{t}^{acc}+1} - P^X_{\tilde{t}^{acc}+1} = 0 \end{cases} \tag{A.3}$$

$$\vdots$$

$$\vdots$$

Therefore, $P_t^X \geq P^{acc}$ when $\tilde{t}^{acc} \leq t \leq \tilde{t}^{acc} + 1$, forcing the amount of bought power to be at least equal to the amount offered in the previous $\tilde{N}^{int}$ intervals. Similar considerations can be done for the discharging power.

References

[1] Wu Y-K, Tang K-T. Frequency support by BESS – review and analysis. Energy Procedia 2019;156:187–91.

[2] Gerini F, Zuo Y, Gupta R, Zecchino A, Yuan Z, Vagnoni E, et al. Optimal grid-forming control of battery energy storage systems providing multiple services: Modeling and experimental validation. Electr Power Syst Res 2022;212:108567. http://dx.doi.org/10.1016/j.epsr.2022.108567.

[3] Zuo Y, Yuan Z, Sossan F, Zecchino A, Cherkaoui R, Paolone M. Performance assessment of grid-forming and grid-following converter-interfaced battery energy storage systems on frequency regulation in low-inertia power grids. Sustain Energy Grids Netw 2021;27:100496. http://dx.doi.org/10.1016/j.segan.2021.100496.

[4] Osmose. European long-term scenarios description - D1.1. 2019, p. 25–6.

[5] Vetter J, Novák P, Wagner M, Veit C, Möller K-C, Besenhard J, et al. Ageing mechanisms in lithium-ion batteries. J Power Sources 2005;147(1):269–81. http://dx.doi.org/10.1016/j.jpowsour.2005.01.006.

[6] Schmalstieg J, Käbitz S, Ecker M, Sauer DU. A holistic aging model for Li(NiMnCo)O_2 based 18650 lithium-ion batteries. J Power Sources 2014;257:325–34. http://dx.doi.org/10.1016/j.jpowsour.2014.02.012.

[7] Bloomberg-New-Energy-Finance. New energy outlook 2017. 2017.

[8] Tan Z, Li X, He L, Li Y, Huang J. Primary frequency control with BESS considering adaptive SoC recovery. Int J Electr Power Energy Syst 2020;117. http://dx.doi.org/10.1016/j.ijepes.2019.105588.

[9] Zhang YJA, Zhao C, Tang W, Low SH. Profit-maximizing planning and control of battery energy storage systems for primary frequency control. IEEE Trans Smart Grid 2018;9(2):712–23. http://dx.doi.org/10.1109/TSG.2016.2562672.

[10] Engels J, Claessens B, Deconinck G. Optimal combination of frequency control and peak shaving with battery storage systems. IEEE Trans Smart Grid 2020;11(4):3270–9. http://dx.doi.org/10.1109/TSG.2019.2963098.

[11] Merten M, Olk C, Schoeneberger I, Sauer DU. Bidding strategy for battery storage systems in the secondary control reserve market. Appl Energy 2020;268:114951. http://dx.doi.org/10.1016/j.apenergy.2020.114951.

[12] Perninge M, Eriksson R. Optimal tertiary frequency control in power systems with market-based regulation. In: 20th IFAC world congress. Vol. 50. No. 1. 2017, p. 4374–81. http://dx.doi.org/10.1016/j.ifacol.2017.08.881.

[13] Rancilio G, Bovera F, Merlo M. Revenue stacking for BESS: Fast frequency regulation and balancing market participation in Italy. Int Trans Electr Energy Syst 2022.

[14] Gusev YP, Subbotin PV. Using battery energy storage systems for load balancing and reactive power compensation in distribution grids. In: 2019 ICIEAM. 2019, p. 1–5. http://dx.doi.org/10.1109/ICIEAM.2019.8742909.

[15] Padmanabhan N, Ahmed M, Bhattacharya K. Battery energy storage systems in energy and reserve markets. IEEE Trans Power Syst 2020;35(1):215–26. http://dx.doi.org/10.1109/TPWRS.2019.2936131.

[16] Bosisio A, Moneta D, Vespucci MT, Zigrino S. A procedure for the optimal management of medium-voltage AC networks with distributed generation and storage devices. Procedia - Soc Behav Sci 2014;108:164–86.

[17] Ghazavi Dozein M, Gomis-Bellmunt O, Mancarella P. Simultaneous provision of dynamic active and reactive power response from utility-scale battery energy storage systems in weak grids. IEEE Trans Power Syst 2021;36(6):5548–57. http://dx.doi.org/10.1109/TPWRS.2021.3076218.

[18] Arteaga J, Zareipour H. A price-maker/price-taker model for the operation of battery storage systems in electricity markets. IEEE Trans Smart Grid 2019;10(6):6912–20. http://dx.doi.org/10.1109/TSG.2019.2913818.

[19] Benini M, Canevese S, Cirio D, Gatti A. Battery energy storage systems for the provision of primary and secondary frequency regulation in Italy. In: 2016 IEEE 16th EEEIC. 2016, p. 1–6. http://dx.doi.org/10.1109/EEEIC.2016.7555748.

[20] Canevese S, Gatti A, Micolano E, Pellegrino L, Rapizza M. Battery energy storage systems for frequency regulation: Simplified aging evaluation. In: 2017 6th ICCEP. 2017, p. 291–7. http://dx.doi.org/10.1109/ICCEP.2017.8004830.

[21] Xu B, Oudalov A, Ulbig A, Andersson G, Kirschen DS. Modeling of lithium-ion battery degradation for cell life assessment. IEEE Trans Smart Grid 2018;9(2):1131–40. http://dx.doi.org/10.1109/TSG.2016.2578950.

[22] Karagiannopoulos S, Rigas A, Hatziargyriou N, Hug G, Oudalov A. Battery energy storage capacity fading and control strategies for deterministic and stochastic power profiles. In: 2016 PSCC. 2016, p. 1–7. http://dx.doi.org/10.1109/PSCC.2016.7540956.

[23] Xu B, Zhao J, Zheng T, Litvinov E, Kirschen DS. Factoring the cycle aging cost of batteries participating in electricity markets. IEEE Trans Power Syst 2018;33(2):2248–59. http://dx.doi.org/10.1109/TPWRS.2017.2733339.

[24] ASTM-E1049-85(2017). Standard practices for cycle counting in fatigue analysis. 2017, URL https://compass.astm.org/EDIT/html_annot.cgi?E1049.

[25] Zhang Y, Xu Y, Yang H, Dong ZY, Zhang R. Optimal whole-life-cycle planning of battery energy storage for multi-functional services in power systems. IEEE Trans Sustain Energy 2020;11(4):2077–86. http://dx.doi.org/10.1109/TSTE.2019.2942066.

[26] Abdulla K, de Hoog J, Muenzel V, Suits F, Steer K, Wirth A, et al. Optimal operation of energy storage systems considering forecasts and battery degradation. IEEE Trans Smart Grid 2018;9(3):2086–96. http://dx.doi.org/10.1109/TSG.2016.2606490.

[27] Liu K, Hu X, Yang Z, Xie Y, Feng S. Lithium-ion battery charging management considering economic costs of electrical energy loss and battery degradation. Energy Convers Manage 2019;195:167–79. http://dx.doi.org/10.1016/j.enconman.2019.04.065.

[28] Cheng Y, Tai Y. A MILP model for optimizing distributed resource system with energy storage and PV considering energy storage life loss. In: 2018 2nd IEEE conference on EI2. 2018, p. 1–6. http://dx.doi.org/10.1109/EI2.2018.8582247.

[29] Xu Y, Zhao T, Zhao S, Zhang J, Wang Y. Multi-objective chance-constrained optimal day-ahead scheduling considering BESS degradation. CSEE J Power Energy Syst 2018;4(3):316–25. http://dx.doi.org/10.17775/CSEEJPES.2016.01050.

[30] Khalilisenobari R, Wu M. Optimal participation of price-maker battery energy storage systems in energy and ancillary services markets considering degradation cost. 2020, arXiv:2006.05659.

[31] Petrelli M, Fioriti D, Berizzi A, Poli D. Multi-year planning of a rural microgrid considering storage degradation. IEEE Trans Power Syst 2021;36(2):1459–69. http://dx.doi.org/10.1109/TPWRS.2020.3020219.

[32] Ecker M, Nieto N, Käbitz S, Schmalstieg J, Blanke H, Warnecke A, et al. Calendar and cycle life study of Li(NiMnCo)O_2-based 18650 lithium-ion batteries. J Power Sources 2014;248:839–51. http://dx.doi.org/10.1016/j.jpowsour.2013.09.143.

[33] Schimpe M, Truong CN, Naumann M, Jossen A, Hesse HC, Reniers JM, et al. Marginal costs of battery system operation in energy arbitrage based on energy losses and cell degradation. In: 2018 IEEE EEEIC and 2018 IEEE I CPS Europe. 2018, p. 1–5. http://dx.doi.org/10.1109/EEEIC.2018.8493717.

[34] Park Y-G, Kim C, Park J-B. MILP-based dynamic efficiency scheduling model of battery energy storage systems. J Electr Eng Technol 2016;11:1063–9. http://dx.doi.org/10.5370/JEET.2016.11.5.1063.

[35] Sarker MR, Murbach MD, Schwartz DT, Ortega-Vazquez MA. Optimal operation of a battery energy storage system: Trade-off between grid economics and storage health. Electr Power Syst Res 2017;152:342–9. http://dx.doi.org/10.1016/j.epsr.2017.07.007.

[36] Parthasarathy C, Hafezi H, Laaksonen H. Integration and control of lithium-ion BESSs for active network management in smart grids: Sundom smart grid backup feeding case. Electr Eng 2022;104.

[37] Wang J, Hashemi S, You S, Træholt C. Active and reactive power support of MV distribution systems using battery energy storage. In: 2017 IEEE international conference on industrial technology. 2017, p. 382–7. http://dx.doi.org/10.1109/ICIT.2017.7913261.

[38] Adewuyi OB, Shigenobu R, Ooya K, Senjyu T, Howlader AM. Static voltage stability improvement with battery energy storage considering optimal control of active and reactive power injection. Electr Power Syst Res 2019;172:303–12.

[39] Zhu Y, Liu C, Dai R, Liu G, Xu Y. Optimal battery energy storage placement for transient voltage stability enhancement. In: 2019 IEEE power & energy society general meeting. 2019, p. 1–5. http://dx.doi.org/10.1109/PESGM40551.2019.8973610.

[40] Wang W, He W, Cheng J, Huang X, Liu H. Active and reactive power coordinated control strategy of battery energy storage system in active distribution network. In: 2017 32nd Youth academic annual conference of chinese association of automation. 2017, p. 462–5. http://dx.doi.org/10.1109/YAC.2017.7967453.

[41] Gulotta F, Rossi A, Bovera F, Falabretti D, Galliani A, Merlo M, et al. Opening of the Italian ancillary service market to distributed energy resources: Preliminary results of UVAM project. In: 2020 IEEE 17th Int. Conf. HONET. 2020, p. 199–203. http://dx.doi.org/10.1109/HONET50430.2020.9322822.

[42] Sethi S, Sorger G. A theory of rolling horizon decision making. Ann Oper Res 1991;29:387–416.

[43] Falabretti D, Gulotta F, Siface D. Scheduling and operation of RES-based virtual power plants with e-mobility: A novel integrated stochastic model. Int J Electr Power Energy Syst 2023;144:108604.

[44] Vanderbeck F, Savelsbergh MW. A generic view of Dantzig–Wolfe decomposition in mixed integer programming. Oper Res Lett 2006;34(3):296–306. http://dx.doi.org/10.1016/j.orl.2005.05.009.

[45] de Souza Dutra MD, Alguacil N. Optimal residential users coordination via demand response: An exact distributed framework. Appl Energy 2020;279:115851. http://dx.doi.org/10.1016/j.apenergy.2020.115851.

[46] Reniers J, Mulder G, Howey D. Review and performance comparison of mechanical-chemical degradation models for lithium-ion batteries. J Electrochem Soc 2019;166:A3189–200. http://dx.doi.org/10.1149/2.0281914jes.

[47] Han X, Ouyang M, Lu L, Li J, Zheng Y, Li Z. A comparative study of commercial lithium ion battery cycle life in electrical vehicle: Aging mechanism identification. J Power Sources 2014;251:38–54. http://dx.doi.org/10.1016/j.jpowsour.2013.11.029.

[48] Engels J, Claessens B, Deconinck G. Techno-economic analysis and optimal control of battery storage for frequency control services, applied to the German market. Appl Energy 2019;242:1036–49. http://dx.doi.org/10.1016/j.apenergy.2019.03.128.

[49] TERNA. Procedura per l'approvvigionamento a termine di risorse di dispacciamento per i soggetti titolari di Unità Virtuali Abilitate Miste (UVAM) al Mercato dei Servizi di Dispacciamento. 2020, URL https://download.terna.it/terna/0000/1071/85.PDF.

[50] Gonzalez-Castellanos AJ, Pozo D, Bischi A. Non-ideal linear operation model for li-ion batteries. IEEE Trans Power Syst 2020;35(1):672–82. http://dx.doi.org/10.1109/TPWRS.2019.2930450.

[51] ARERA. Testo integrato del dispacciamento elettrico. 2019.
[52] Snyder RD. Linear programming with special ordered sets. J Oper Res Soc 1984;35(1):69–74.
[53] Zimmerman R, Murillo-Sanchez C. MATPOWER user's manual. 2020, http://dx.doi.org/10.5281/zenodo.4074122.
[54] Bisschop J. Optimization modelling. 2020.
[55] Hu Y-C, Lin M-H, Carlsson JG, Ge D, Shi J, Tsai J-F. A review of piecewise linearization methods. Math Probl Eng 2013. http://dx.doi.org/10.1155/2013/101376.
[56] Guha A, Patra A. State of health estimation of lithium-ion batteries using capacity fade and internal resistance growth models. IEEE Trans Transp Electrif 2018;4(1):135–46. http://dx.doi.org/10.1109/TTE.2017.2776558.
[57] Mandli A, Kaushik A, Patil R, Naha A, Hariharan K, Kolake S, et al. Analysis of the effect of resistance increase on the capacity fade of lithium ion batteries. Int J Energy Res 2019;43. http://dx.doi.org/10.1002/er.4397.
[58] NHOA-ENERGY. Battery, inverter and transformer data-sheets. 2021.
[59] Kim T-J, Kang D-W, Lee Y-H, Hyun D-S. The analysis of conduction and switching losses in multi-level inverter system. In: IEEE 32nd annual power electronics specialists conference. Vol. 3. 2001, p. 1363–8. http://dx.doi.org/10.1109/PESC.2001.954310.
[60] Chen Z, Yuan L, Zhao Z, Sun X. Power losses in two- and three-level three phase photovoltaic inverters equipped with IGBTs. In: 15th ICEMS. 2012, p. 1–6.
[61] Kolar J, Zach F, Casanellas F. Losses in PWM inverters using IGBTs. In: Electric power applications, IEEE proceedings. Vol. 142. 1995, p. 285–8. http://dx.doi.org/10.1049/ip-epa:19952018.
[62] Kuczma M. Introduction to the theory of functional equations and inequalities: Cauchy's equation and Jensen's inequality. 2009, p. 1–595. http://dx.doi.org/10.1007/978-3-7643-8749-5.
[63] Fitzgerald AE, Kingsley C, Umans S. Electric machinery. McGraw-Hill Education; 2002.
[64] GME. Electricity markets data. 2020, URL https://www.mercatoelettrico.org/it/Mercati/MercatoElettrico/MPE.aspx.